



Temperature dependence of magnetic hysteresis

Yongjae Yu and Lisa Tauxe

Geosciences Research Division, Scripps Institution of Oceanography, 9500 Gilman Drive, Department 0220, La Jolla, California 92093-0220, USA (ltauxe@ucsd.edu; yjyu@ucsd.edu)

Bruce M. Moskowitz

Institute for Rock Magnetism, University of Minnesota, 310 Pillsbury Drive SE, Minneapolis, Minnesota 55455, USA (bmosk@umn.edu)

[1] Hysteresis measurements have become a routine procedure in characterizing the magnetic remanence carriers of rocks. In this study we have investigated the temperature dependence of magnetic hysteresis in order to better recognize the dominant anisotropy and changes of domain state at various temperatures. Hysteresis properties have been measured at a series of temperatures between 20 K and 873 K for synthetic magnetites and natural (titano)magnetite-bearing samples. For synthetic samples and gabbros, shape anisotropy dominates most temperature ranges, while magnetocrystalline anisotropy controls hysteresis properties below 120 K. Titanomagnetite-bearing oceanic basalts show quite different behavior with much higher coercivity, resulting from prominent magnetostrictive anisotropy. While many factors such as composition, field treatment, grain shape and size, and stress affect hysteresis properties at various temperature ranges, a dominant anisotropy was better recognized when remanence ratio was plotted against coercivity.

Components: 8845 words, 15 figures, 2 tables.

Keywords: coercivity; day plot; hysteresis; magnetite; remanence ratio.

Index Terms: 1518 Geomagnetism and Paleomagnetism: Magnetic fabrics and anisotropy; 1540 Geomagnetism and Paleomagnetism: Rock and mineral magnetism; 1599 Geomagnetism and Paleomagnetism: General or miscellaneous.

Received 23 December 2003; **Revised** 5 April 2004; **Accepted** 30 April 2004; **Published** 19 June 2004.

Yu, Y., L. Tauxe, and B. M. Moskowitz (2004), Temperature dependence of magnetic hysteresis, *Geochem. Geophys. Geosyst.*, 5, Q06H11, doi:10.1029/2003GC000685.

Theme: Geomagnetic Field Behavior Over the Past 5 Myr

1. Introduction

[2] In environmental magnetism and paleomagnetism, measuring magnetic hysteresis has become a routine process in characterizing remanence carriers of rocks. In general, values of M_s (saturation magnetization), M_r (saturation remanence), and B_c (coercivity) are determined from hysteresis loops after appropriate nonferrimagnetic slope correction.

On the other hand, values of B_{cr} (coercivity of remanence) are obtained from back-field measurements. In practice, these parameters or their ratios provide useful information on the domain states and, by implication, the average grain size of the remanence carriers.

[3] Knowledge of the temperature dependence of hysteresis properties is useful in deciphering

Table 1. Synthetic Samples^a

Powder	d, μm	q (Axial Ratio)	n
4000	0.065	1.48	884
5099	0.21	1.44	1300
Mapico	0.24	1.29	532
5000	0.34	1.65	1262
112978	0.44	1.33	1022
3006	1.06	1.62	1471
112982	16.9	1.61	1618

^a Powders 4000, 5000, 112978, 3006, and 112982 are from the Wright Company. Powders 5099 and Mapico are the products of Pfizer and Mapico Companies. d is the estimated grain size, q is the average axial ratio, and n is the number of grains counted. Size distribution was determined by counting individual grains from at least six different SEM photos per powder. See Yu *et al.* [2002] for details.

dominant anisotropy. In addition, changes of domains structures at high/low temperatures can be recognized and interpreted. Although the low-temperature hysteresis properties of titanomagnetites have been extensively studied [Tucker, 1981; Schmidbauer and Schembera, 1987; Argyle and Dunlop, 1990; Hodych, 1990; Schmidbauer and Keller, 1996; Moskowitz *et al.*, 1997; Hodych *et al.*, 1998; Muxworthy, 1999; Özdemir, 2000; Kostrov, 2001, 2002; Smirnov and Tarduno, 2002; Özdemir *et al.*, 2002], the high-temperature hysteresis properties of (titano)magnetites have been relatively less studied [Levi and Merrill, 1978; Özdemir and O'Reilly, 1981, 1982; Hartstra, 1982a, 1982b; Beske-Diehl and Soroka, 1984; Dunlop, 1987; Heider *et al.*, 1987; Bina and Prevot, 1989; Argyle and Dunlop, 1990; Schmidbauer and Keller, 1994; Keller and Schmidbauer, 1999].

[4] In most previous studies, a systematic low- and high-temperature hysteresis has not been measured. In this study we will investigate the temperature dependence of hysteresis properties on well-documented (titano)magnetites. The present study was intended to report hysteresis measurements made on the same magnetites at temperatures ranging from low (20–30 K) to above the Curie temperature (853 K) of magnetites. These data provide valuable constraints on what the dominant anisotropies at various temperatures for each sample are.

2. Samples and Experiments

[5] Seven synthetic powders were studied whose mean grain sizes range from single domain (SD;

65 nm) to small multidomain (MD; 16.9 μm). A brief summary of sample properties is presented in Table 1 (see Yu *et al.* [2002] for detailed sample description). For each grain size, three sets of powders were prepared. The first set of powders is 0.5% by volume dispersions of magnetite in a matrix of CaF_2 . These were vacuum sealed in quartz capsules of 3 cm and annealed for 3 hours at 973 K to stabilize the magnetic properties. After annealing, samples were slowly cooled from 973 K because rapid quenching may result in higher thermal stresses. The quartz capsules were unsealed just prior to hysteresis measurements. The second set of powders is 0.5% by volume dispersions of unannealed magnetite in a matrix of CaF_2 . The third set consists of undispersed, pure magnetite powders.

[6] Natural samples were also studied: CG (Cordova Gabbro, Ontario, Canada [Yu and Dunlop, 2002]); KM (Kometsuka basalts, Mt. Aso, Japan [Yu, 1998]); MORB 1–7 (zero-age mid-oceanic ridge basalts, East Pacific Rise [Gee and Kent, 1999]); SBG (submarine basaltic glass, ODP 807C [Pick and Tauxe, 1993]); and TG-A and TG-B (Tudor Gabbro, Ontario, Canada [Yu and Dunlop, 2001]) (Table 2). On the basis of previous studies, we selected individual chips whose sister chips yielded hysteresis ratios falling in various regions in the Day plot [Day *et al.*, 1977], spanning the range from single domain, pseudo single domain (PSD), multidomain, and superparamagnetic (SP). In particular, MORB 1–7 represents subsamples spaced every 5 mm with respect to the outer chilled margin of a single pillow lava with MORB 1 representing a subsample nearest the chilled margin. We anticipate SP/SD behavior for MORB 1 and 2 and SD/PSD behavior for MORB 3–7 [see Gee and Kent, 1999, Figure 5].

Table 2. Natural Samples^a

Sample	References	T_{UB} , $^{\circ}\text{C}$
Basaltic Glass	1	300–520
Cordova Gabbro	2	550–580
Kometsuka Basalt	3	500–560
MORBs	4	160–360
Tudor Gabbro	5	580

^a T_{UB} is the maximum unblocking temperatures from the thermal demagnetization of sister specimens. References: 1, Pick and Tauxe [1993]; 2, Yu and Dunlop [2002]; 3, Yu [1998]; 4, Gee and Kent [1999]; 5, Yu and Dunlop [2001].

[7] As a sample selection process, room temperature hysteresis was measured for at least eight chips per sample or per powder by using the alternating gradient force magnetometer (AGFM) at Scripps. For selected chips we have determined the temperature dependence of hysteresis using low- and high-temperature vibrating sample magnetometers (VSMs). In addition, one set of low-temperature hysteresis loops was measured using a Quantum Design MPMS-2 SQUID magnetometer system. All the temperature-dependent measurements were carried out at the Institution for Rock Magnetism, University of Minnesota.

[8] Hysteresis loops were measured in the peak field of 1 T in field increments of 10 mT. The signal averaging time was usually set to 200 ms, but 1 s was used for weak samples. Hysteresis was measured at various temperatures from 20 K to 873 K. These temperature ranges include the Verwey transition T_v (119–121 K), room temperature T_0 (298 K), and the Curie point T_c (853 K) of magnetite. In order to maintain thermal equilibrium, temperature was varied with a rate of 1°C per 6 s. Below T_0 , temperature intervals were 20 K, whereas above T_0 the temperature interval was 40 K. For a few samples of special interest, finer temperature intervals were used.

[9] In most samples, hysteresis loops were not entirely saturated, particularly at very low temperatures (<100 K). In this temperature range a different nonferrimagnetic slope correction was required. Among various correction techniques, we followed an approach suggested by *Kosterov* [2002]. Average values of M_s were estimated for the interval of $\mu_0 H = 0.75$ – 0.95 T, where M_s varied 1–6%. Note that we used a saturation field of $\mu_0 H = 1$ T. Despite this correction, underestimation of M_s is unavoidable, resulting in overestimation of squareness, as evidenced in some natural samples whose M_r/M_s was higher than 0.5.

[10] For natural samples the same chips were used for both low- and high-temperature measurements. For these chips, low-temperature hysteresis was measured first, before subjecting them to any high-temperature treatment. For synthetic samples, different chips (but from the same

batch) were used for low- and high-temperature runs.

[11] Synthetic samples and natural gabbros show little sign of alteration during the high-temperature experiments. We checked their reproducibility by monitoring hysteresis during heating and cooling cycles. None of these samples show more than 5% discrepancy of their hysteresis parameters at a given temperature. In particular, temperature dependence of hysteresis for gabbros was monitored through triple heating-cooling cycles from T_0 to T_c , yielding virtually indistinguishable outcomes. This high thermal stability was anticipated because their remanence carriers are elongated magnetites encapsulated within silicates [*Yu and Dunlop*, 2001, 2002]. However, basaltic samples show signs of alteration during heat treatment. We usually measured the temperature dependence of hysteresis for three chips of each natural sample. For basaltic samples the best hysteresis results from the chip that showed minimal alteration are presented.

[12] To compare our results with those in the literature, B_{cr} was also measured. However, because it involves additional measurements separate from the hysteresis loop measurement, B_{cr} was obtained only for selected samples. All the hysteresis results are listed in Table A1¹ (low-temperature results) and Table A2 (high-temperature results).

3. Results

3.1. Hysteresis Loops

[13] For convenience, all the measured loops or estimated parameters will be compared to those at room temperature. Representative examples of hysteresis loops are presented in Figure 1. Although the full hysteresis loop was measured, only the trimmed portion of the descending loops for $-0.1 < \mu_0 H < 0.5$ T is shown for clarity (Figure 1).

[14] For synthetic samples we used different chips for low- and high-temperature measurements (Figures 1a and 1b). For these samples, magnetization is nearly saturated by 0.1 T as the temper-

¹Auxiliary material is available at <ftp://ftp.agu.org/apend/gc/2003GC000685>.

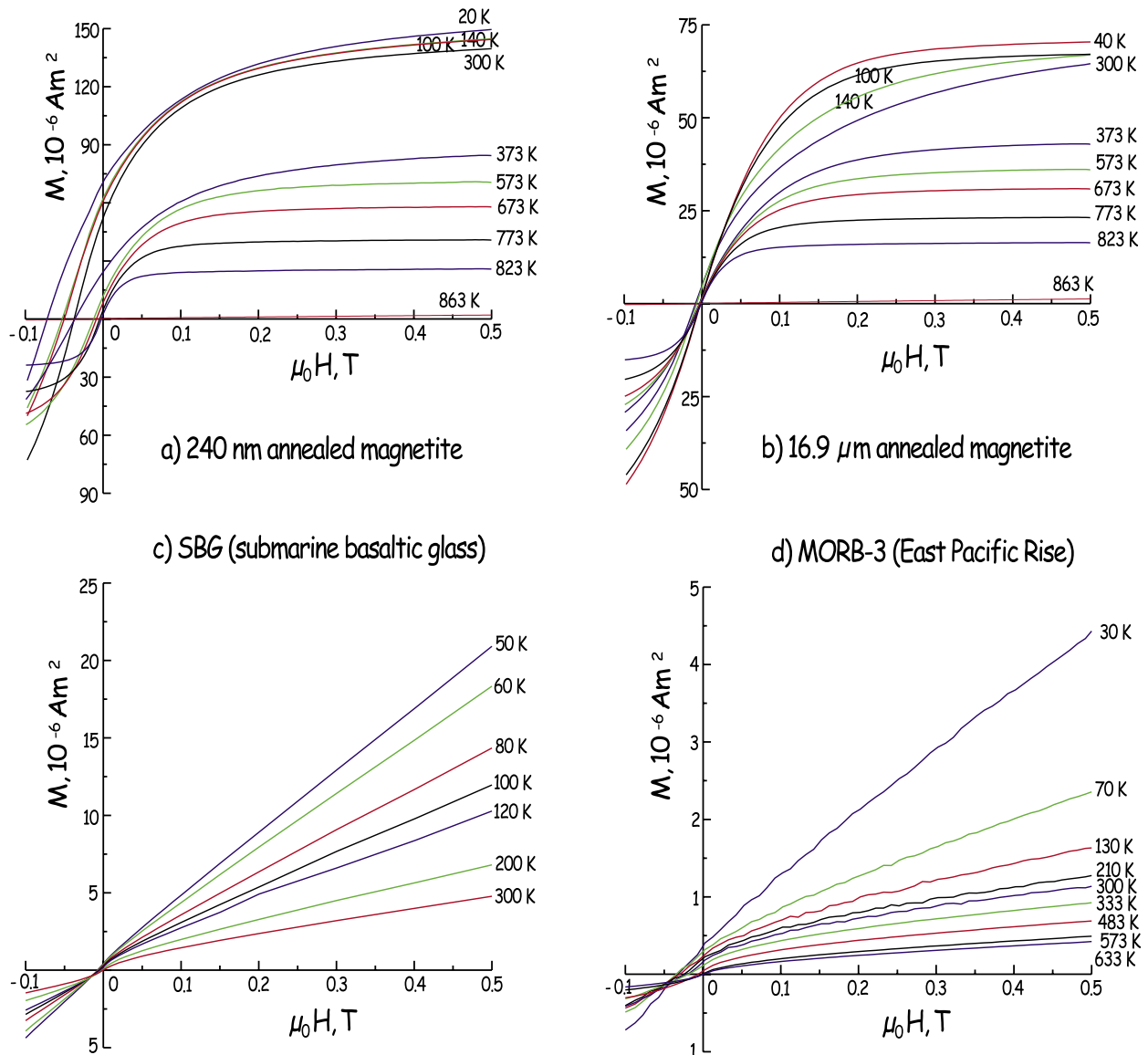


Figure 1. Descending branches of hysteresis loops determined at various temperatures. For convenience, only the trimmed portion, $-0.1 < \mu_0 H < 0.5$ T, is illustrated: (a) 240 nm magnetite, (b) 16.9 μm magnetite, (c) SBG (submarine basaltic glass), and (d) MORB-3 (mid-ocean ridge basalt, East Pacific Rise).

ature increases above T_0 . After passing T_c (853 K), the loops become paramagnetic. For 240 nm magnetite, loops measured at 100 K and 140 K are virtually indistinguishable despite the intervening Verwey transition (Figure 1a). In contrast, loops for 16.9 μm magnetite at 100 K and at 140 K approach saturation at slightly different rates (Figure 1b).

[15] Natural samples show a quite different behavior. Most noticeably, the paramagnetic contribution of the matrix is dominant for SBG and MORB

samples (Figures 1c and 1d), producing nearly linear M - $\mu_0 H$ behavior at low temperatures. In addition, for MORB samples this type of behavior extends throughout the entire temperature range of 600 K (Figure 1d).

3.2. High-Temperature Hysteresis: Synthetic Samples

[16] Typical temperature dependences of the hysteresis parameters (M_s , M_r , and B_c) are compared

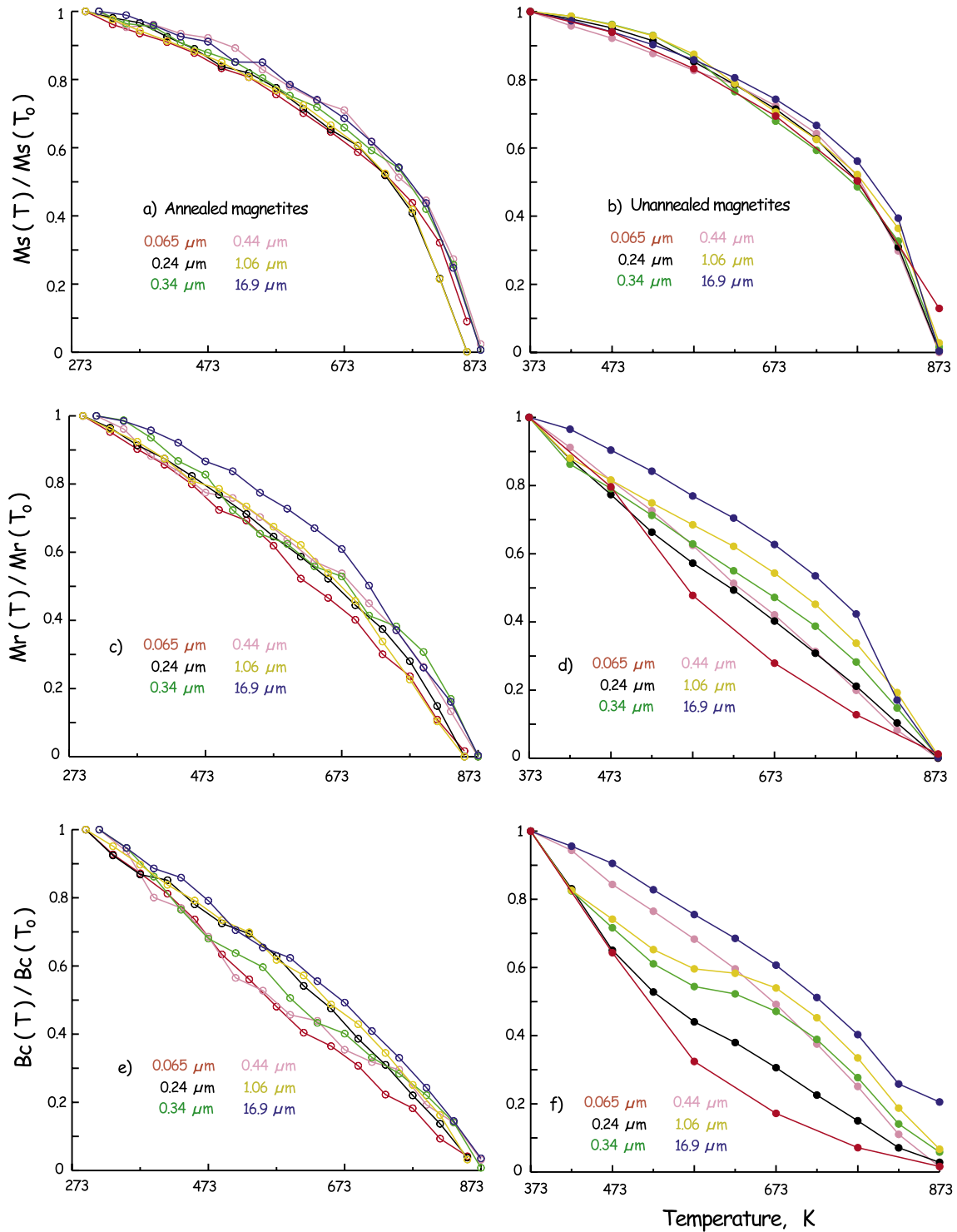


Figure 2. Temperature dependences of hysteresis properties for synthetic samples. (a and b) $M_s(T)$, (c and d) $M_r(T)$, and (e and f) $B_c(T)$. Results for annealed (left side) and unannealed (right side) powders are illustrated separately. M_s , M_r , and B_c all decrease as temperature increases.

for all the synthetic powders used in this study (Figure 2). As expected, annealed (open symbols) and unannealed (solid symbols) powders show similar temperature dependence of M_s (Figures 2a and 2b). M_r and B_c all decay more rapidly with temperature than M_s (Figures 2c–2f). We also observed that M_r decreases slightly less rapidly than B_c in most samples. These observations agree with those of Dunlop [1987] but are different from those of Levi and Merrill [1978].

[17] Regardless of grain size, annealed samples show a monotonic decay of M_s , M_r , and B_c (Figure 2, left side). On the other hand, for unannealed samples, finer grains show temperature intervals of much more rapid decay of M_r and B_c (Figure 2, right side).

[18] The squareness ($=M_r/M_s$) is a well-known indicator of domain structure. The temperature dependence of squareness is illustrated, showing that smaller grains possess higher remanence over the entire temperature range (Figure 3a). In a given grain size, the annealed set maintains lower squareness than the unannealed set except for the SD sample at high temperatures (Figure 3a). B_{cr} was monitored only for the annealed magnetites. Temperature dependence of B_{cr} is similar to that of B_c (Figure 3b). In a Day diagram, hysteresis ratios appear to migrate toward what is known as the MD region as temperature increases (Figure 3c).

[19] We summarize our results in the squareness-coercivity (SC) plot [Tauxe et al., 2002]. In an SC plot, annealed and unannealed powders follow slightly different paths (Figures 4a and 4b). Unannealed magnetites sweep out broader regions because their initial squareness and coercivity at T_0 were larger owing to the effect of stress. In addition, most annealed samples show an inflection near 813–833 K (Figure 4), below which squareness rapidly decreases toward the (super)paramagnetic origin (zero remanence and zero coercivity).

3.3. High-Temperature Hysteresis: Natural Samples

[20] We plot the high-temperature hysteresis parameters for natural samples in Figure 5. As temperature increases, all the hysteresis parameters

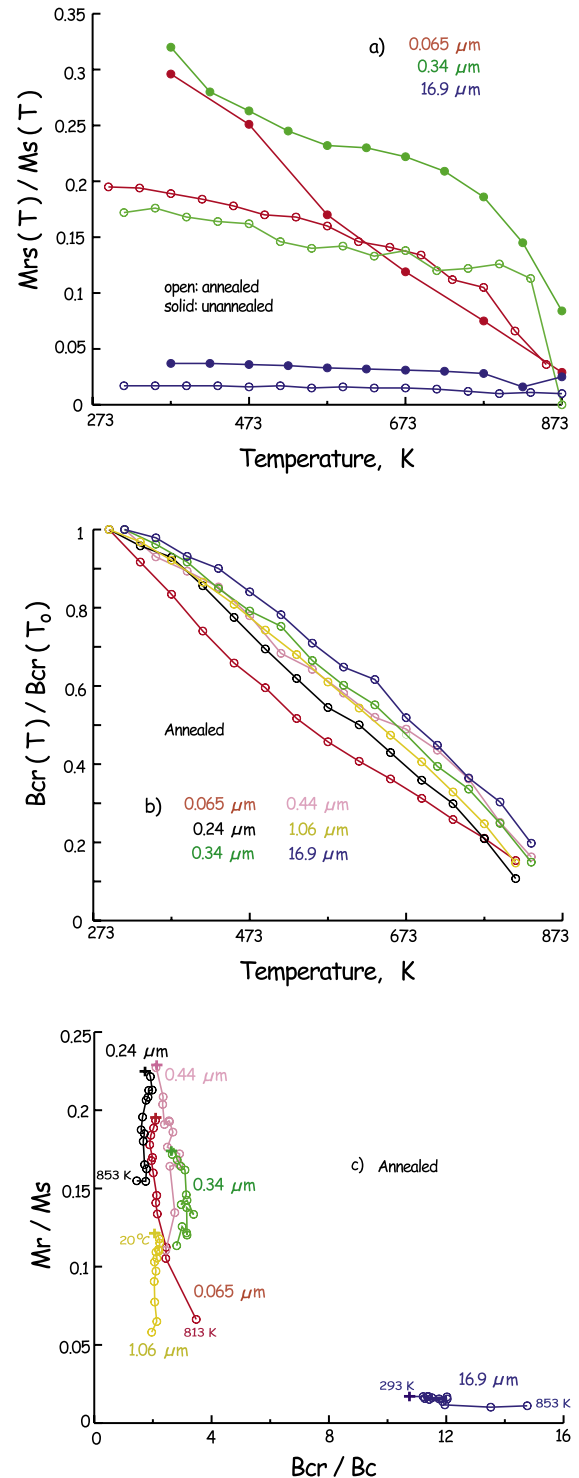


Figure 3. (a) Examples of measured temperature dependence of squareness. Except for 65 nm magnetite at high temperatures, unannealed magnetite shows higher squareness. (b) Measured temperature dependence of B_{cr} for annealed powders. (c) A Day diagram for annealed magnetites. Plus signs are the room temperature measurements.

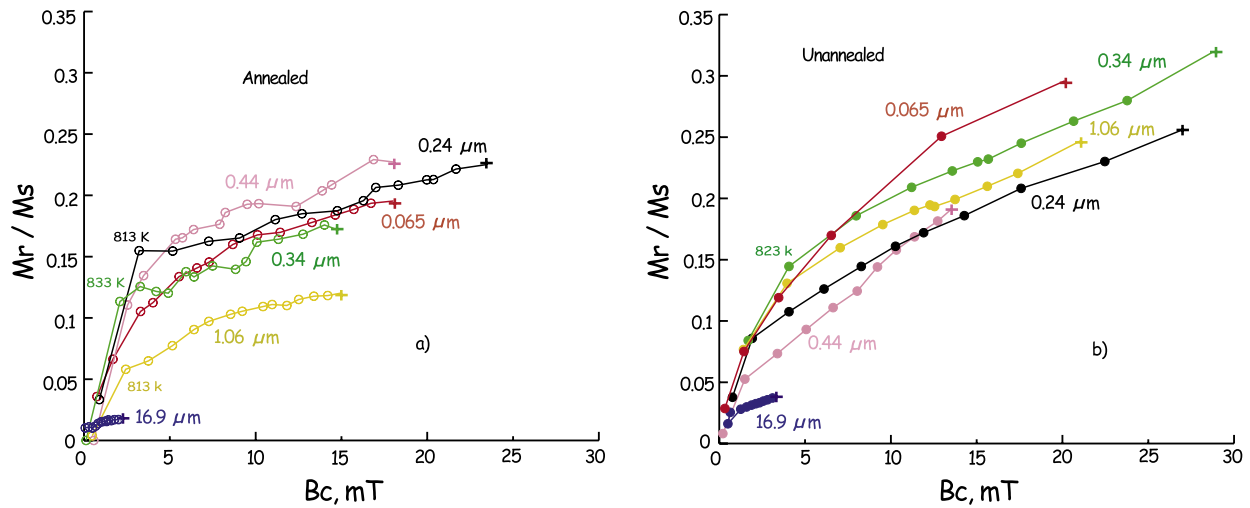


Figure 4. Hysteresis results for synthetic magnetites in SC plots (a) for annealed magnetites and (b) for unannealed magnetites. As the temperature increases, squareness and coercivity migrate toward the (super)paramagnetic origin of zero remanence and zero coercivity.

decrease. B_c decays the most rapidly, followed by B_{cr} and M_r , while M_s decays the least rapidly (Figure 5). These trends are similar to those observed in the synthetic magnetite samples. In particular, basaltic samples show fairly rapid decay for all their hysteresis parameters (Figures 5b, 5d, 5f, and 5h). In these samples, M_s decays almost linearly with temperatures, while B_c , B_{cr} , and M_r decay somewhat quasi-exponentially.

[21] Despite the distinctly different temperature dependences between magnetite- and titanomagnetite-bearing samples (Figure 5), they are quite similar to each other in SC plots (Figures 6a and 6b) and in Day diagrams (Figures 6c and 6d). In general, results for MORBs reach slightly smaller squareness than those for magnetite-bearing samples and spread toward much higher coercivities (Figure 6b).

3.4. Low-Temperature Hysteresis: Synthetic Samples

3.4.1. Effect of Annealing, Field Cooling, and Volume Concentration

[22] It has been well documented that hysteresis properties are dependent on many factors, such as composition, field cooling, grain shape and size, initial demagnetization states, stress, and volume concentration. We used synthetic samples to inves-

tigate these effects. For 0.24 μm , 1.06 μm , and 16.9 μm magnetites, three sets (annealed 0.5%, unannealed 0.5%, unannealed bulk) of magnetites were subjected to temperature dependence of hysteresis under two different conditions, zero field cooled (ZFC) and field cooled (FC) in a large field of 1 T [Moskowitz *et al.*, 1993]. As each sample is cooled down to the next temperature interval, a 1 T field was applied for the FC state. For the ZFC state, the stray field was no more than 1 μT (J. Marvin, personal communication, 2003). Overall, for each grain size, six different data sets were obtained (Figure 7).

[23] For PSD samples, as temperature decreases, annealed powders show a drastic increase in their B_c , B_{cr} , and M_r below T_v (Figures 7a–7e). However, unannealed powders show rather small increases in B_c and M_r . Furthermore, their increases occur over a broad temperature range, compared to the sharp increase near T_v for annealed samples. Regardless of the annealing condition and volume concentration, there is also an interesting trend that increases in B_c are prominent in ZFC, while increases in M_r are prominent in FC for submicron magnetites (Figure 7). B_{cr} steadily increases as temperature decreases to T_v and then B_c decreases in further cooling (Figure 7c). The drastic increase of B_{cr} below T_v for SD/PSD samples diminishes for MD samples (Figure 7h).

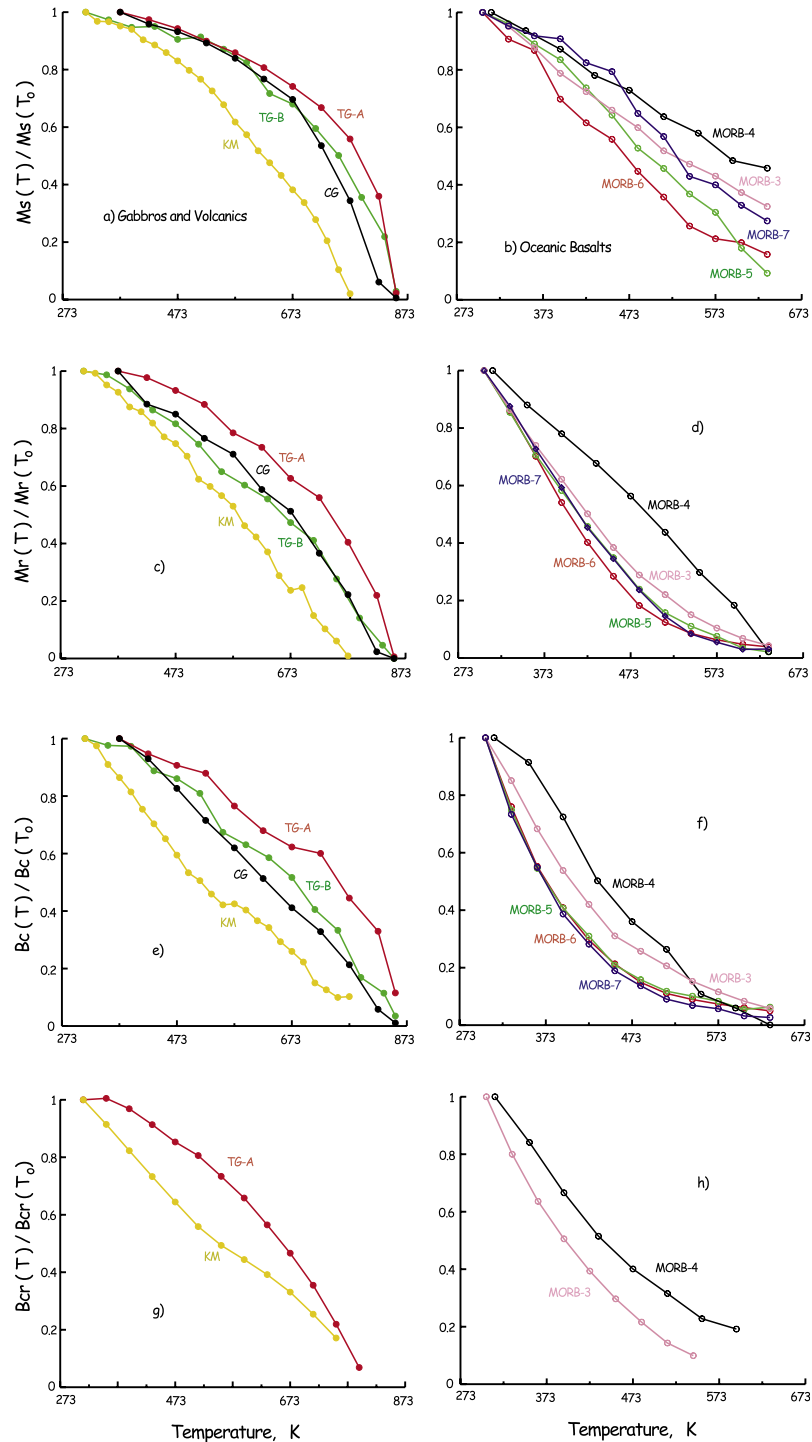


Figure 5. Temperature dependences of hysteresis properties for natural samples. (a and b) $M_s(T)$, (c and d) $M_r(T)$, (e and f) $B_c(T)$, and (g and h) $B_{cr}(T)$. Results for annealed (Figures 5a, 5c, 5e, and 5g) and unannealed (Figures 5b, 5d, 5f, and 5h) powders are illustrated separately. Compared to the results for gabbros and volcanics, hysteresis parameters for oceanic basalts decay rapidly.

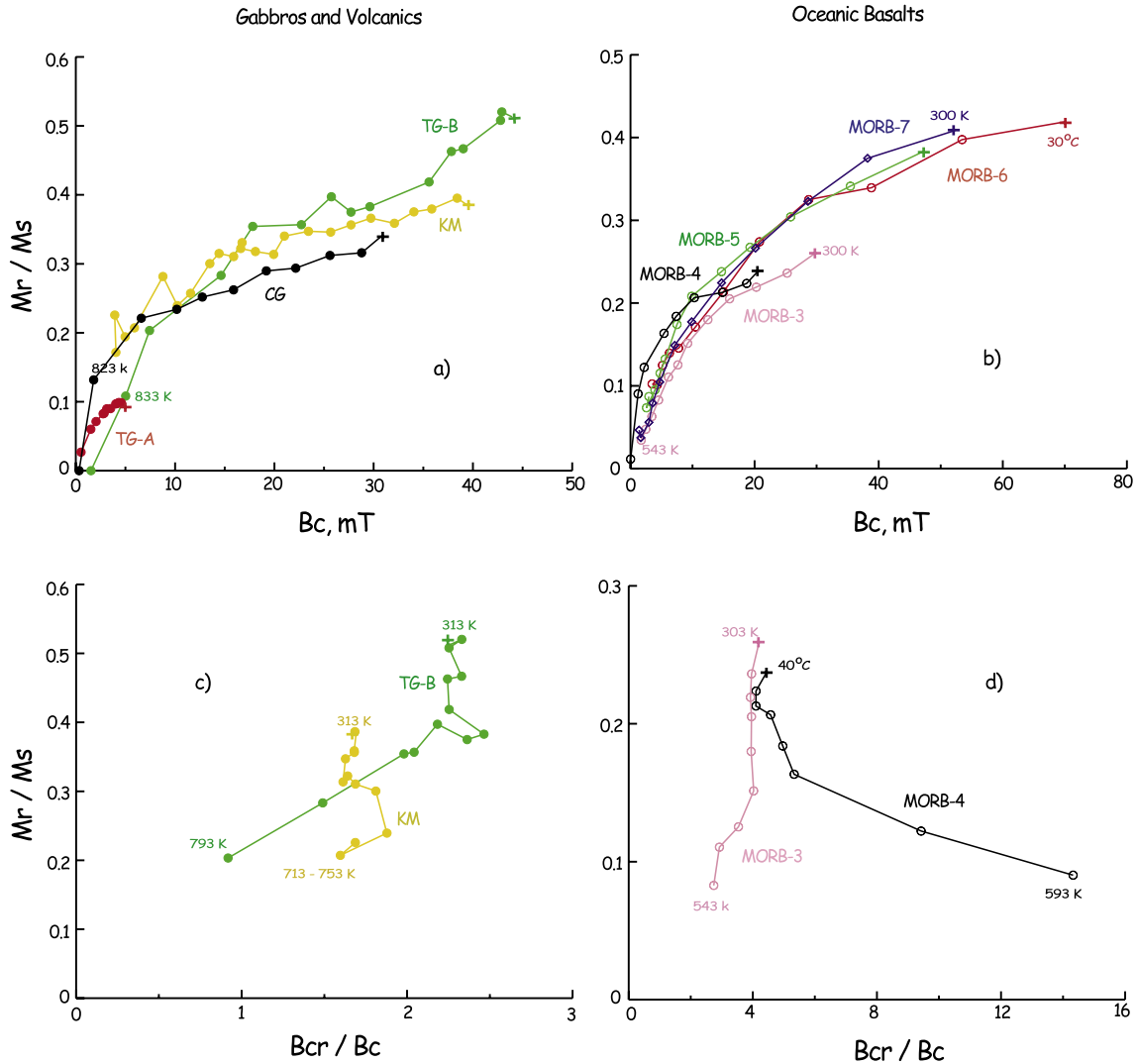


Figure 6. Hysteresis results for natural gabbros and volcanics: (a) an SC plot, (b) a Day diagram, (c) an SC plot, and (d) a Day diagram for oceanic basalts. Plus signs are the room temperature measurements. Note that oceanic basalts (Figures 6c and 6d) spread toward higher coercivities than magnetite-bearing samples (Figures 6a and 6b).

[24] In SC plots the effect of annealing, ZFC/FC, and volume concentration on PSD magnetites is clearly demonstrated (Figures 8a and 8c). The effect of annealing reduces stress, giving rise to smaller squareness. In particular, results for 0.24 μm and 1.06 μm are surprising (Figures 8a and 8c). Values of squareness at T_0 for the annealed samples lie in the lower limit of PSD values (squareness equals 0.05), while those for unannealed powders lie at 0.23–0.38. In these powders, values of B_c for annealed and unannealed samples at 30 K are different by about a factor of 2. The absence of an applied field during cooling through the Verwey transition

causes much higher coercivity but less remanence, resulting in a different migration path with a steeper route for FC (Figures 8a and 8c). Compared to other factors, the effect of volume concentration makes the least distinction for 0.24 μm and 1.06 μm (Figures 8a and 8c). Bulk unannealed powders show higher squareness with slightly larger B_c than 0.5% unannealed magnetites. The reported effects of annealing [Lowrie and Kent, 1969; Dankers and Sugiura, 1981] and volume concentration [Dankers and Sugiura, 1981; Dankers, 1981; Schmidbauer and Keller, 1994] at T_0 are in good agreement with our observations. All of these observations are,

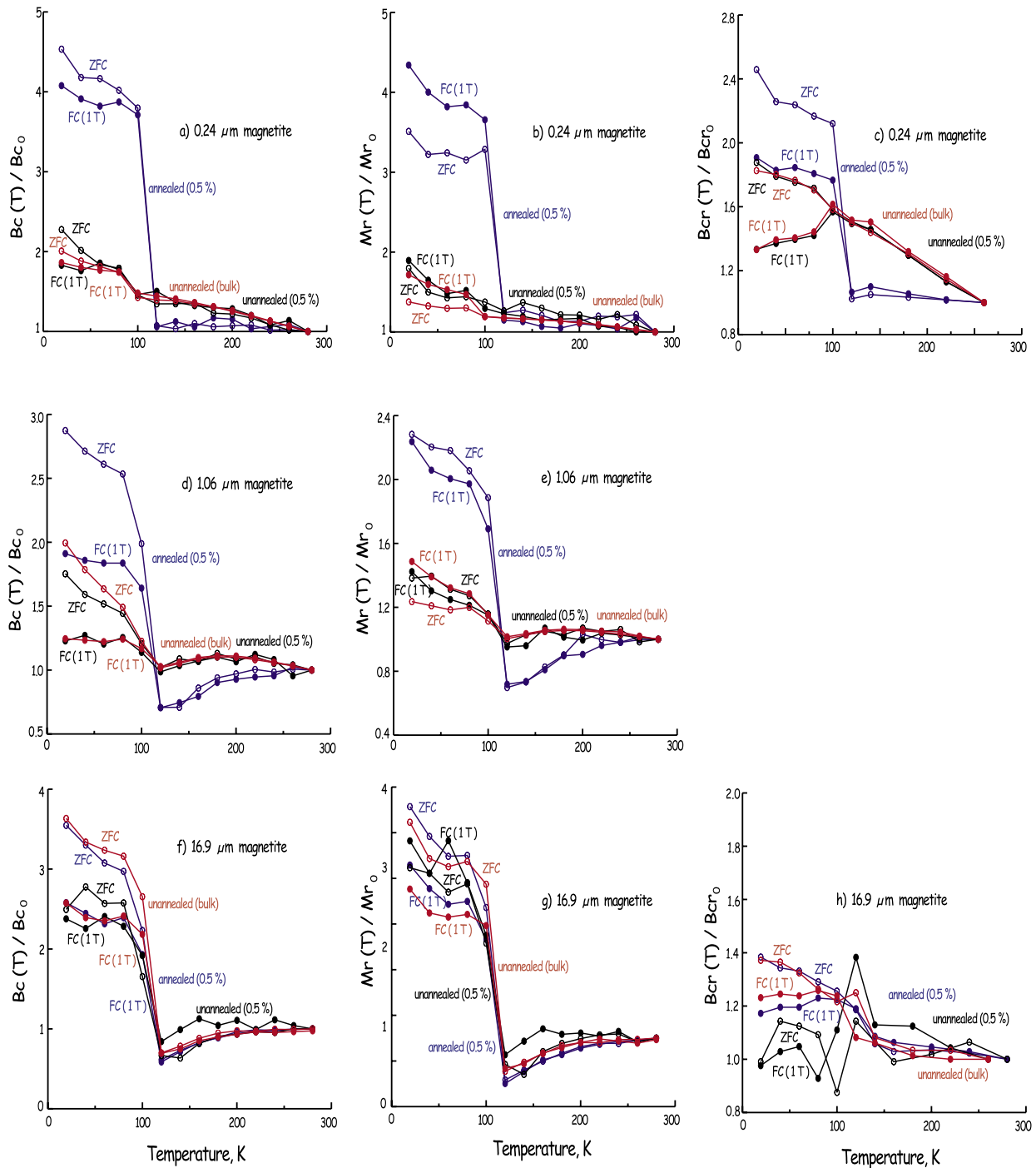


Figure 7. Effect of annealing, field cooling, and volume concentration on hysteresis properties: (a–c) 0.24 μm magnetite, (d and e) 1.06 μm magnetite, and (f–h) 16.9 μm magnetite. The low-temperature transition of magnetite is prominent for the annealed magnetite set.

however, less clear when the results are displayed in a Day diagram for 0.24 μm magnetites (Figure 8b). For example, the effects of volume concentration and FC/ZFC are hard to resolve (Figure 8b).

[25] Results for MD grains show four unique aspects. First, below T_v , values of B_c , B_{cr} , and M_r were usually higher for ZFC than for FC (Figures 7f–7h). Note that values of M_r were

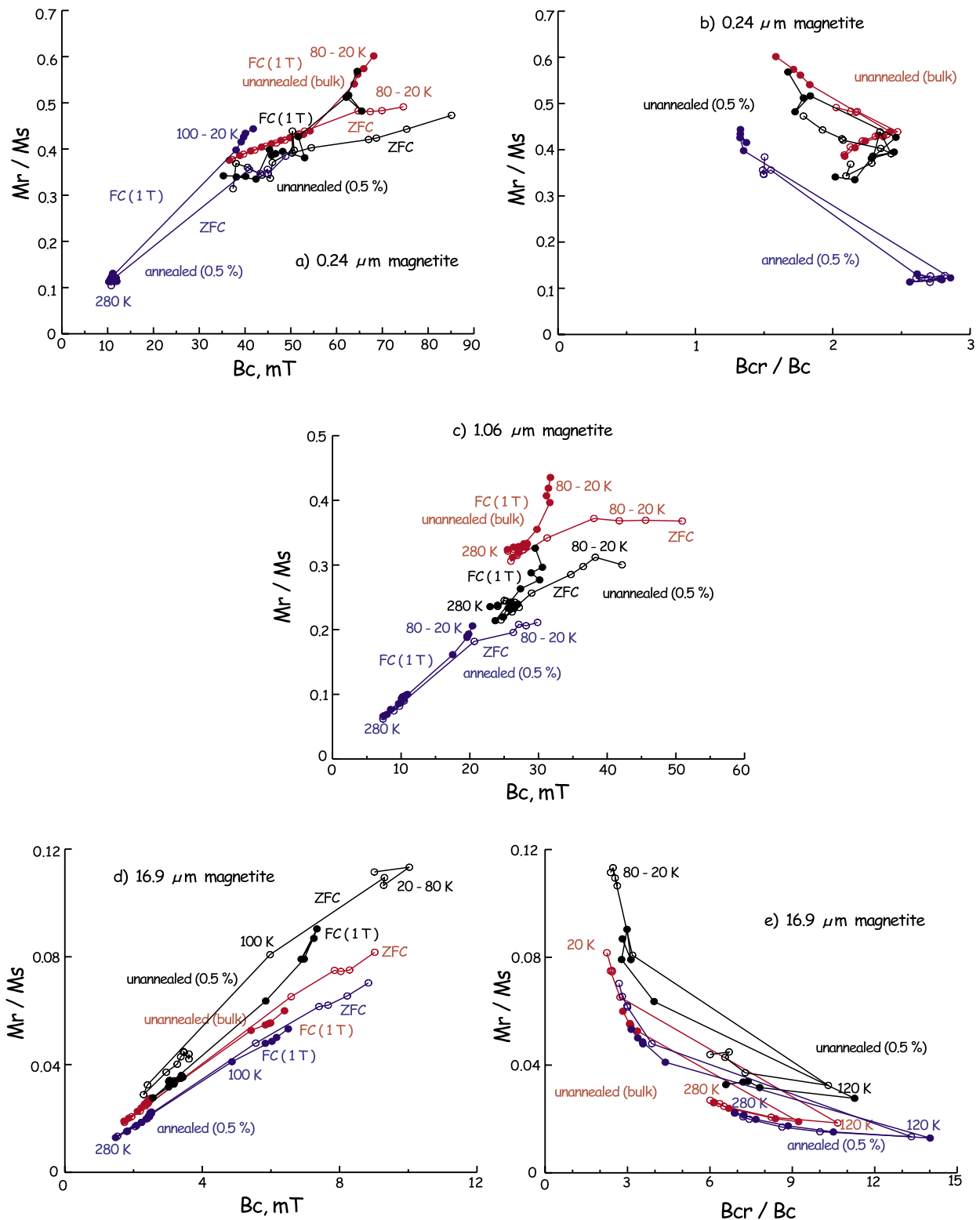


Figure 8. The SC plots for (a) 0.24 μm , (c) 1.06 μm , and (d) 16.9 μm magnetites. The Day diagrams for (b) 0.24 μm and (e) 16.9 μm magnetites.

higher for submicron magnetites in FC condition (Figures 7b and 7e). Second, in an SC plot, results for unannealed 0.5% magnetite lie above those for unannealed bulk powders, implying that a higher volume concentration actually decreases their MD remanence (Figure 8d). This trend is exactly the opposite of that for PSD samples. Third, the existence of an applied field during cooling controls the temperature dependence of hysteresis the most (Figure 8d). Fourth, as temperature decreases, hysteresis parameters migrate along a prograde-retrograde path (Figures 8d and 8e). They evolve toward a more MD-like region (lower squareness and coercivity) to 120 K and then migrate back up toward higher squareness and coercivity below 120 K.

3.4.2. Temperature Dependence of Hysteresis Properties

[26] Temperature dependence of three hysteresis parameters (B_c , B_{cr} , and M_r) is plotted in Figure 9. All of the parameters were normalized to those measured at T_0 . As temperature decreases, B_c and M_r decrease slightly with minima near T_v for 1.06 μm and 16.9 μm magnetites, beyond which both parameters abruptly jump to higher values. However, submicron magnetites do not show a steady decrease from T_0 to 120 K. After the jumps near 120 K, B_c , B_{cr} , and M_r steadily increase as temperature decreases further. The magnitude of the jumps near T_v shows no obvious grain size dependence for all parameters (Figure 9). For all annealed magnetites, jumps were higher for ZFC states than for FC states for B_c (Figures 9a and 9b), but exactly the opposite trend is observed for M_r (Figures 9c and 9d). Temperature dependence of M_s is not presented because M_s remained relatively constant with only a slight increase at very low temperatures. As a result, the temperature dependence of M_r/M_s is mainly controlled by variation of M_r (Figure 10).

[27] For the four selected powders (0.065 μm , 0.24 μm , 0.44 μm , and 16.9 μm), B_{cr} measurements were carried out as well (Figures 9e and 9f). In traditional Day plots, hysteresis parameters migrate toward higher values of squareness and lower values for B_{cr}/B_c as temperature decreases

(Figures 10c and 10d). In a given grain size, hysteresis results make no clear distinction between ZFC versus FC except that values of FC reach slightly higher squareness owing to the easy axis bias during field cooling (Figures 10c and 10d).

[28] Much more rock magnetic information can be deduced from SC plots (Figures 10a and 10b), which reveal two intriguing trends. First, the evolution of B_c shows a grain size dependence. An MD grain covers <10 mT, while SD-PSD powders span up to 30–60 mT. It is somewhat surprising that this simple grain size dependence holds for both ZFC and FC states (Figures 10a and 10b). Second, for SD/PSD samples the hysteresis results above T_v are very similar between FC and ZFC states, but they diverge below T_v (Figure 10b). Below T_v , ZFC data form a concave-down shape (quadratic), while FC follows a concave-up shape (parabolic). At a given temperature, FC data achieve a higher remanence with a lower B_c than ZFC (Figures 10a and 10b).

3.5. Low-Temperature Hysteresis: Natural Samples

[29] Temperature dependence of B_c , B_{cr} , and M_r for natural samples behaves quite differently than the synthetic samples (Figure 11). Magnetite-bearing gabbros show an increase of B_c and M_r below 110 K (Figures 11a, 11c, and 11e). However, the jumps near 110 K are less prominent than those for annealed synthetic samples and occur over a broad temperature range. For Cordova Gabbro (CG), the results for ZFC and FC are virtually identical, indicating that exposure to applied fields during cooling makes no impact (Figures 11a and 11c).

[30] Results from submarine basaltic glass (SBG) and MORBs are different. First of all, as temperature decreases, the hysteresis parameters continuously increase over the entire temperature range without showing any sudden jumps (Figures 11b, 11d, and 11f). Second, some samples show 20 to 80 times increase of B_c (Figure 11b). Thermal blocking of SP grains into SD states would explain this large increase.

[31] We measured B_{cr} for SBG, five MORBs, and TG-A. In Day plots, two distinct trends are shown

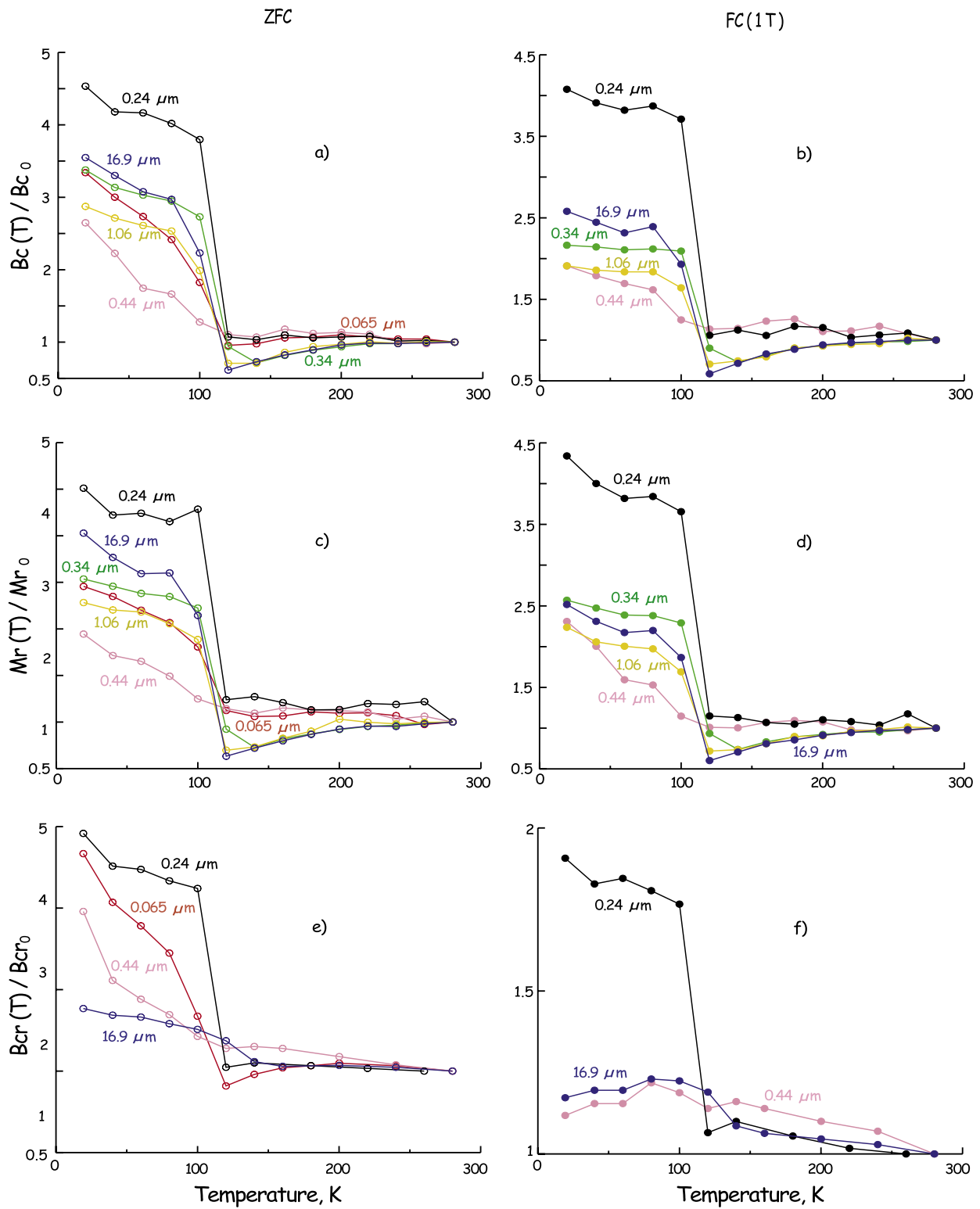


Figure 9. Temperature dependences of hysteresis properties for annealed synthetic samples: (a and b) $B_c(T)$, (c and d) $M_r(T)$, and (e and f) $B_{cr}(T)$. Results for zero field cooled (Figures 9a, 9c, and 9e) and field cooled (Figures 9b, 9d, and 9f) are illustrated separately. The 0.24 μm magnetite shows the largest increase of hysteresis properties below 120 K.

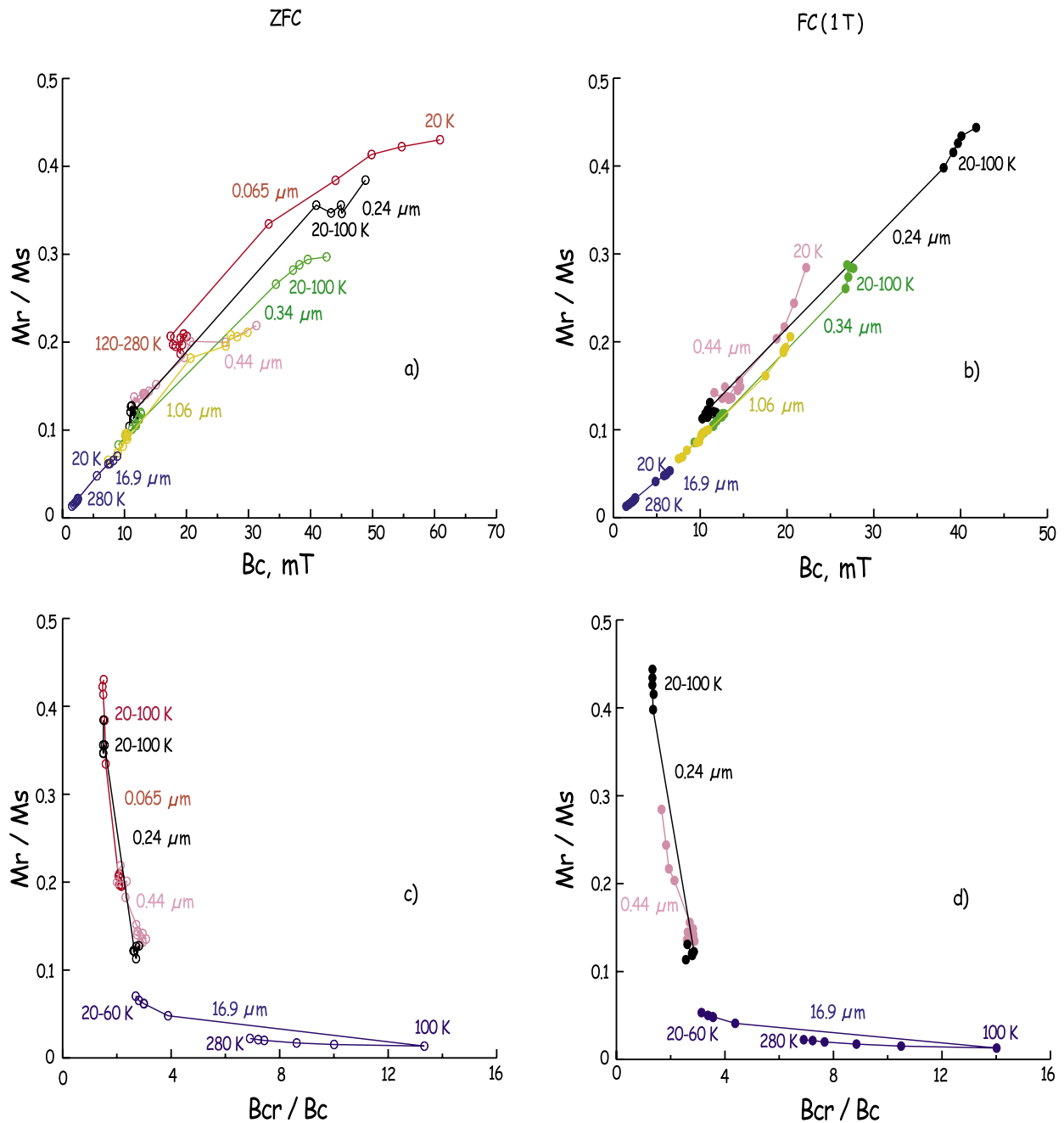


Figure 10. Hysteresis results for synthetic annealed samples: (a) an SC plot for ZFC, (b) an SC plot for FC, (c) a Day diagram for ZFC, and (d) a Day diagram for FC. Note that zero-field-cooled and field-cooled data sets follow different paths on SC plots, which is hardly recognizable in conventional Day plots.

(Figures 12b and 12d). The results for TG-A fall along the typical PSD-MD trend, while those for MORBs follow the trend of SP+SD mixture. Such a difference was anticipated because natural samples used in this study have different grain sizes as well as different compo-

sition. These trends are also visible in SC plots (Figures 12a and 12c). Results from CG have maximum coercivity of 70 mT at 30 K. On the other hand, results for SBG and MORBs follow a different path with surprisingly high coercivity. In MORB samples a B_c of 100 mT is quite common

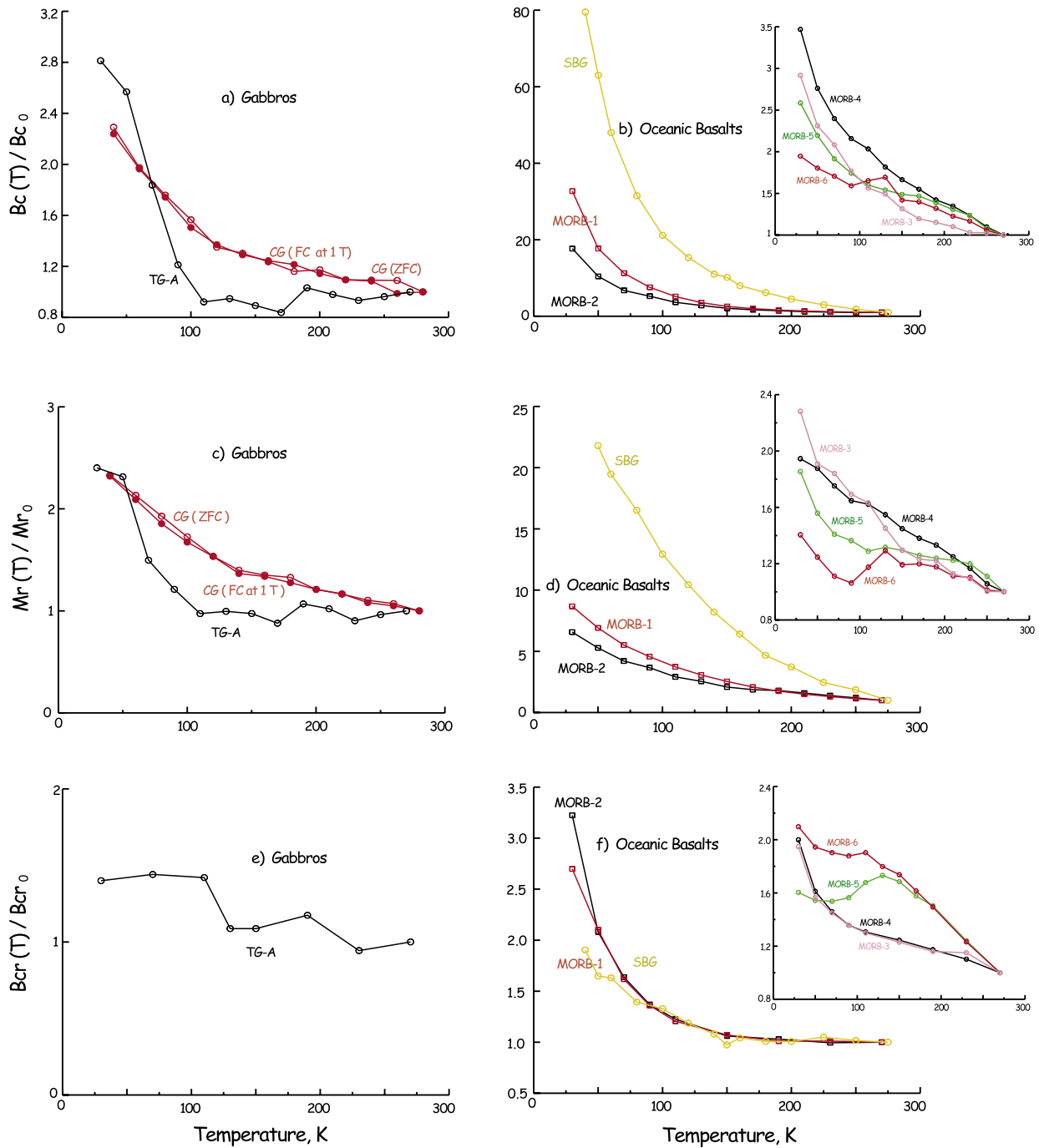


Figure 11. Temperature dependences of hysteresis properties for natural samples: (a and b) $B_c(T)$, (c and d) $M_r(T)$, and (e and f) $B_{cr}(T)$. Results for gabbros (Figures 11a, 11c, and 11e) and oceanic basalts (Figures 11b, 11d, and 11f) are illustrated separately. Because of gigantic scale difference, results for MORBs are illustrated as insets.

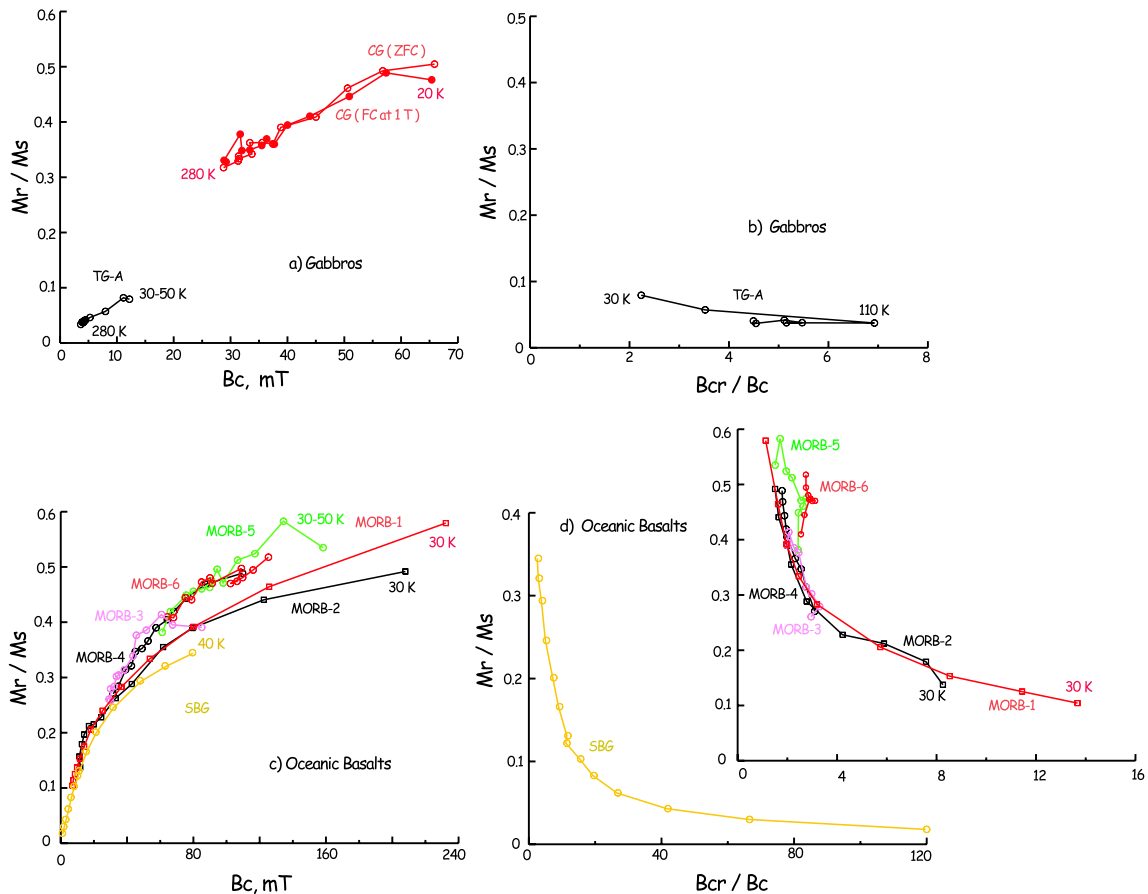


Figure 12. Hysteresis results for natural gabbros and volcanics: (a) an SC plot, (b) a Day diagram, (c) an SC plot, and (d) a Day diagram for oceanic basalts. Because of gigantic scale difference, results for MORBs are illustrated as insets.

at low temperature, often reaching over 200 mT (Figure 12c).

3.6. Effect of Sample's Manufacturer for Synthetic Powders

[32] Hysteresis properties for 0.21 μm magnetite, manufactured by Pfizer Company, are distinct from other powders of similar grain size. At high temperature ranges, hysteresis parameters for 0.21 μm magnetite decay less rapidly than those for 0.24 μm magnetite (Figure 13). Grain size/shape cannot be the source of this difference because a nominal axial ratio of 1.44 for 0.21 μm magnetite is not very different from other powders (Table 1). It is interesting that 0.21 μm magnetite behaves more MD-like with smaller squareness and coercivity than 0.24 μm magnetite (Figures 15a and 15b).

[33] The 0.21 μm magnetite also shows a unique behavior at low temperatures (Figures 14 and 15c). Bulk unannealed samples show higher squareness than 0.5% unannealed set, which is exactly the opposite of all other synthetic powders. It is currently unclear why this particular magnetite behaves differently. Perhaps the different synthetic processes from the manufacturer are responsible.

4. Discussion

4.1. High-Temperature Results

[34] Hysteresis at any given temperature is mostly controlled by three competing physical energies. In many natural and synthetic samples, magnetostatic effects such as self-demagnetization and shape anisotropy dominate magnetic particles. When internal stresses are high, magnetostrictive energy

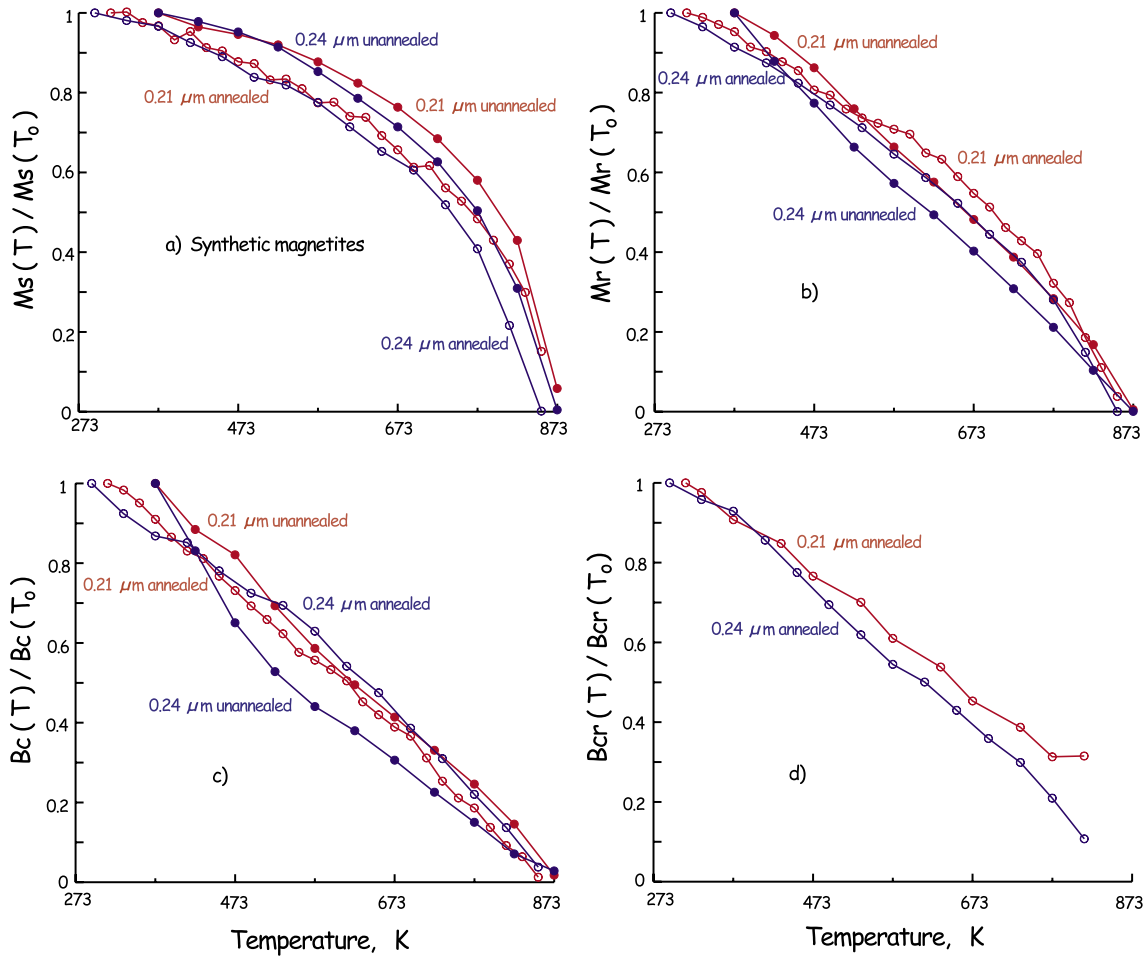


Figure 13. Comparison of temperature dependences of hysteresis for 0.21 μm (Pfizer Company) and 0.24 μm (Mapico Company) magnetites: (a) $M_s(T)$, (b) $M_r(T)$, (c) $B_c(T)$, and (d) $B_{cr}(T)$. Two magnetites behave quite differently, strongly suggesting that the consistency in sample preparation is as important as physical properties of magnetites.

can be important. Magnetostriction is the variation in the dimensions of a magnetic grain under the influence of the applied field. Magnetocrystalline anisotropy is the least important factor at higher temperatures for (titano)magnetite because of its rapid decay with temperature. Magnetocrystalline energy is the difference between two magnetic energies acquired along the easy and hard axes of the crystal. In general, we anticipate that shape anisotropy would dominate for synthetic samples because all the samples have axial ratios greater than 1.3 (Table 1).

[35] The dominant anisotropy at higher temperatures has been recognized by estimating a power law dependence of B_c with M_s [see Dunlop, 1987,

and references therein]. For dominant magneto-crystalline and magnetoelastic anisotropy, B_c varies as λ/M_s and K/M_s [Fletcher and O'Reilly, 1974; Moskowitz, 1993], where λ is the magnetoelastic constant and K is the magnetocrystalline constant. On the other hand, B_c follows the trend of $M_s(T)$ for dominating shape anisotropy. For example, λ and K vary as $M_s(T)$ to the power of 2.5 and 8–9 for magnetites [Klapel and Shive, 1974; Moskowitz et al., 1993]. In $\text{Fe}_{2.4}\text{Ti}_{0.6}\text{O}_4$, λ and K decrease as $M_s^3(T)$ and $M_s^6(T)$ [Moskowitz et al., 1993; Sahu and Moskowitz, 1995].

[36] The temperature dependence of B_c and M_r shows interesting trends for unannealed magnetites (Figures 2d and 2f). Unannealed samples show a

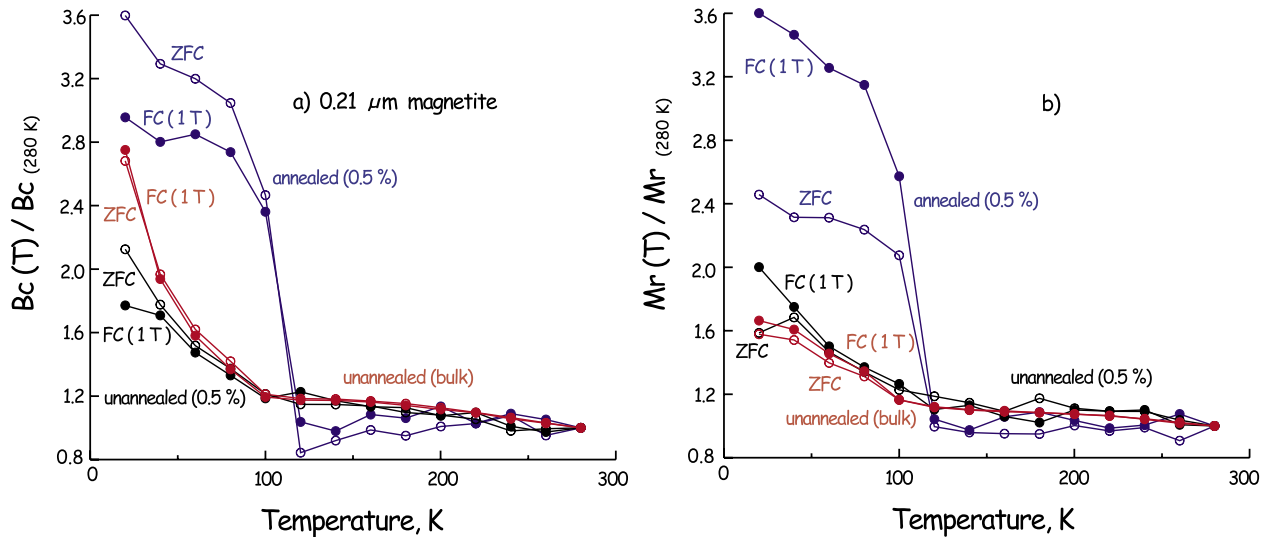


Figure 14. Effect of annealing, field cooled, and volume concentration on hysteresis properties of 0.21 μm magnetites: (a) $B_c(T)$ and (b) $M_r(T)$.

pronounced grain size dependence. As grain size decreases, B_c and M_r decay more rapidly. For annealed magnetites, $B_c = M_s^{1.8} - M_s^{2.2}$, indicating that the shape anisotropy as well as the effect of thermal fluctuation [Dunlop, 1977] are important factors controlling B_c . The increasing contribution of stress is responsible for the higher power dependence of unannealed magnetites. In particular, B_c of unannealed SD magnetite shows significantly higher power dependence of M_s , $B_c = M_s^{5.4}$.

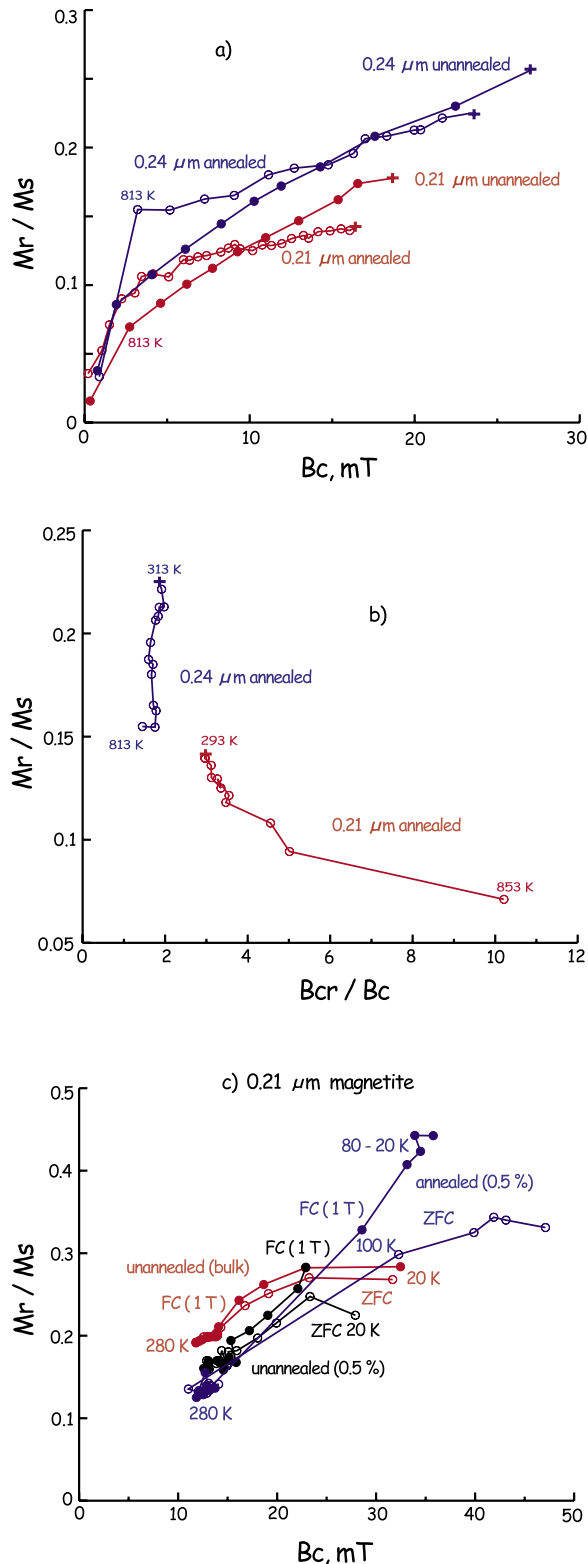
[37] In SC plots, hysteresis parameters of annealed and unannealed samples migrate along different paths as temperature increases (Figure 4). First, at a given temperature, annealed samples show lower squareness and coercivity than the unannealed set, resulting from their reduced stress, with the exception of 0.44 μm magnetite. Second, annealed samples exhibit an inflection near 813–833 K, below which squareness decreases less rapidly than unannealed powders (Figure 4).

[38] Following a flattened path on an SC diagram is anticipated for shape-anisotropy-dominated samples. For PSD samples, values of M_r/M_s can be approximated by $M_r = H_c/N$, where N is a self-demagnetizing factor. When shape anisotropy dominates, H_c and M_s vary with temperature with the same power. By combining these two relations, we get a nearly constant squareness for the entire

range of B_c . This simple approximation holds most of the temperature range for annealed magnetites, where magnetostrictive contribution is minimal (Figure 4a). The final dive into the origin above 813–833 K can be attributed as an increasing contribution of thermal fluctuation, rendering formerly stable remanence transforming into SP (Figures 4a and 4b).

[39] Results for natural samples clearly demonstrate that hysteresis properties of magnetite-carrying samples have quite different temperature dependences than those for titanomagnetite-bearing samples (Figure 5). All of the hysteresis parameters decay rapidly for MORBs. It is interesting that B_c , M_r , and M_s for TG-A ($M_r/M_s = 0.10$ at T_0) decay less rapidly than those for TG-B ($M_r/M_s = 0.51$ at T_0). Rapidly decaying hysteresis parameters for finer grains were also observed for unannealed synthetic samples (Figures 2b, 2d, and 2f). This observation should be taken into account in future rock magnetic theories and micromagnetic modeling.

[40] Temperature dependence of M_s for MORBs indicates that samples are oxidizing as we increase temperatures (Figure 5b). Despite this limitation, in SC plots, results for titanomagnetite-bearing MORBs form the trends of slightly smaller remanence with much higher coercivity than those for



magnetite-bearing gabbros (Figure 6b). It is likely that the much higher values of B_c for MORBs are resulting from a substantial magnetostrictive contribution. Note that magnetostrictive energy is a major contributor to coercivity in Ti-rich titanomagnetite at T_0 [Sahu and Moskowitz, 1995].

4.2. Low-Temperature Results

[41] The interpretations for high-temperature behavior cannot be translated directly into the low-temperature results because of the complicating effect of the temperature dependence of K (the magnetocrystalline anisotropy constant), which changes sign approximately at the isotropic point T_i [Syono and Ishikawa, 1963; Kakol et al., 1991]. Magnetite also experiences a phase transition at the Verwey transition T_v , T_i and T_v are 135 K and 119–121 K for stoichiometric magnetites, respectively.

[42] Hysteresis results for both natural and synthetic samples show a strong temperature dependence. As temperature decreases from T_0 to below T_v , squareness increases (Figures 8, 10, and 12). In some samples, squareness approaches 0.5, the ideal value for SD-like behavior when uniaxial anisotropy dominates [Stoner and Wohlfarth, 1948]. In particular, for annealed synthetic samples, the SC plot serves as a granulometric indicator with higher B_c as grain size decreases (Figures 10a and 10b).

[43] For synthetic samples, results for ZFC and FC follow quite different paths in SC plots (Figures 10a and 10b). Most of all, they tend to diverge below T_v . Below T_v , results for ZFC migrate toward higher coercivity but less squareness than FC for SD/PSD magnetite. The opposite behavior is observed for MD magnetite (16.9 μm). Since M_s shows little sign of temperature dependence, the temperature dependence of M_r and B_c was solely responsible. Indeed, at a given temperature, ZFC samples reached higher values of B_c but lower

Figure 15. Comparison of temperature dependences of hysteresis for 0.21 μm and 0.24 μm magnetites using (a) an SC plot and (b) a Day diagram; (c) an SC plot for low-temperature hysteresis results for 0.21 μm . Plus signs are the room temperature measurements. It is interesting that 0.21 μm magnetite shows much smaller squareness/coercivity than 0.24 μm magnetite.

values of M_r than FC (1 T) (Figure 9). These trends are universal for all SD/PSD grains for both annealed and unannealed samples (Figures 7–10). A similar FC/ZFC dependence was reported for synthetic PSD magnetites [Kosterov, 2001, 2002; Smirnov and Tarduno, 2002].

[44] Below T_v , the only physical difference between ZFC and FC is the easy axis bias in the FC state. On cooling through T_v , one of the cube edges of the high-temperature cubic phase becomes the monoclinic c axis, which is also the new magnetic easy axis. When an applied field is present during cooling through T_v , the field restricts the c axis to the one of the three cube edges closest to the direction of the applied field. As a result of the restricted choice, the FC sample achieves higher remanence. However, its soft B_c is difficult to explain. One explanation is the existence of ordered monoclinic twins, rendering domain walls less likely to move [e.g., Kosterov, 2002]. But then, this would make B_c harder.

[45] Existence of a monoclinic twin phase is also unclear. Recent advances in imaging techniques based on magnetic force microscopy [Moloni *et al.*, 1996], synchrotron radiation X-ray maps [Medrano *et al.*, 1999], or Bragg diffraction [Baruchel *et al.*, 2001] generally confirm the existence of a monoclinic phase. However, these imaging results were obtained from millimeter-sized magnetites, limiting their generalization on submicron magnetites [see also Kosterov, 2002]. In fact, the smallest size of magnetite where the formation of twin domains has been cited is above 5 μm [Medrano *et al.*, 1999]. Detection of monoclinic twin domains for submicron magnetite is a necessary step in solving this puzzle.

[46] It is anticipated that annealing reduces stress, giving rise to much lower squareness and B_c at T_0 . Results follow the prediction over the entire temperature range studied (Figures 7 and 8). Increasing the volume concentration leads to stronger interaction, resulting in an increase in squareness as well as B_c (Figures 7 and 8). However, this trend is reversed for 16.9 μm magnetites (Figure 8d), indicating that interaction is less important for MD. Another surprise is the

existence of a dichotomy between ZFC and FC regardless of annealing condition or volume concentration (Figure 8).

[47] The 16.9 μm magnetite is quite unique in four respects, two of which have already been discussed but are summarized briefly. First, it shows higher values of B_c and M_r for ZFC to below T_v (Figures 7f and 7g). Second, the increase of volume concentration decreased squareness and B_c (Figures 8d and 8e). Third, a small dip at T_v is visible for all 16.9 μm magnetite, regardless of their annealed states and volume concentration (Figures 7f and 7g), suggesting that annealing was ineffective in eliminating stress. Note also that the increase of B_c and M_r for 16.9 μm at below T_v was not as significant as those for PSD samples. Fourth, both in SC plots and in Day diagrams, hysteresis parameters migrate toward the MD region (lower remanence and coercivity) at first and then migrate in the opposite direction (Figures 8d and 8e). A steady decrease of B_c and M_r while maintaining equal M_s at 300–160 K causes apparent migrations toward MD state.

[48] What is the dominant anisotropy at low temperatures? On the basis of the axial ratios (i.e., greater than 1.3) for synthetic samples, a dominant shape anisotropy was expected over other competing anisotropies. Because shape anisotropy is mainly dependent on M_s , which is almost temperature independent at low temperatures, shape anisotropy would be hardly temperature dependent. Both B_c and M_r were indeed nearly constant for submicron magnetites from T_0 to 120 K, indicating a dominant shape anisotropy (Figure 9). However, B_c and M_r decreased on cooling from T_0 to 120 K for 1.06 μm and 16.9 μm , reaching a minimum at 120 K, following a sudden jump below 120 K.

[49] All of our synthetic PSD magnetites show drastic increases of B_c and M_r below T_v (Figures 7 and 9). Two observations are particularly interesting. First, B_c and M_r show a drastic jump near T_v not near T_i , where values of cubic K change sign and become zero. Second, values of B_c remained almost constant near T_i even though K_1 approaches zero. Among possible sources of anisotropy ener-

gies, temperature dependence of the cubic and monoclinic magnetocrystalline anisotropy constants [Syono and Ishikawa, 1963; Abe et al., 1976; Kakol et al., 1991] fits our results the best in terms of the magnitude of jumps for B_c and M_r . The magnetocrystalline anisotropy becomes much larger than the shape anisotropy only at T_v , despite the fact that K_1 (cubic) becomes zero at T_i . For the temperature intervals between T_v and T_i , shape anisotropy is still dominating. Note that temperature dependence of the cubic and monoclinic magnetocrystalline constants shows a drastic jump on cooling through T_v [e.g., see Abe et al., 1976]. Overall, for PSD samples, shape anisotropy controls the hysteresis properties in the cubic phase (above T_i). As the temperature decreases, this cubic phase first experiences a substantial change at T_i , but at T_v the large increase in magnetocrystalline anisotropy becomes the controlling factor.

[50] Unfortunately, this interpretation works only for magnetite-bearing samples. Hysteresis results for MORBs lack a low-temperature Verwey transition but show continuous increases of B_c , B_{cr} , and M_r as temperature decreases (Figure 11). In these samples a strong thermal dependence of magnetostrictive energy is responsible for their different behavior [Moskowitz et al., 1998; Kosterov, 2002]. In addition, quenching from SP to SD is another likely source that changes their magnetic properties drastically (Figure 11).

[51] Results for CG offer another mystery in our understanding of hysteresis behavior. Contrary to synthetic samples, there is no difference between ZFC and FC in B_c and M_r (Figures 11a and 11c). At first glance it is likely that a high aspect ratio of magnetites in CG [Yu and Dunlop, 2002] is responsible for this interesting behavior. However, this is at odds with the recent theoretical modeling [Carter-Stiglitz et al., 2002], which shows a remanence transition at T_v even for an infinitely elongated grain. An alternative solution would be a compositional difference since even small amounts of nonstoichiometry or minor cations would suppress T_v while hardly affecting T_c . Intensive microprobing on CG magnetites detected combined minor elements (Si and Mg) of no more than 2% [Yu and Dunlop, 2002], which might help

to suppress the Verwey transition and explain the remanence results (Figure 11).

4.3. SC Plots Versus Day Diagrams

[52] Following Day et al. [1977], it is now common to plot the remanence ratio or squareness (M_r/M_s) versus the coercivity ratio (B_{cr}/B_c). In some cases the Day plot has diagnosed different domain states such as MD, PSD, SD, SP, or mixtures of them [Day et al., 1977; Gee and Kent, 1995, 1999; Tauxe et al., 1996; Dunlop, 2002a, 2002b; Fabian, 2003; Lanci and Kent, 2003]. In spite of these successes, there still exist data sets that are beyond the scope of conventional interpretation (e.g., Figure 4) [Tauxe et al., 2002]. This ambiguity results mostly from the fact that hysteresis properties are controlled by many competing factors, such as composition, grain size, grain shape, and stress.

[53] To overcome this uncertainty and to better display hysteresis properties, especially when there is more than an order of magnitude variation on the values of B_c or B_{cr} in a given data set, other plotting schemes were developed by replacing B_{cr}/B_c with either B_c or B_{cr} , namely, a squareness-coercivity (SC) plot or a squareness-remanence coercivity (SRC) plot [Kent and Gee, 1996]. By using an SC plot [Kent and Gee, 1996; Dunlop et al., 1997; Xu et al., 1998; Tauxe and Love, 2003] or SRC plot [Kent and Gee, 1996; Carlot and Kent, 2002], complicated hysteresis properties were better explained. A combined version of the SC and SRC plots was three-dimensionally drawn by plotting squareness versus B_c versus B_{cr} [Borradaile and Lagroix, 2000a, 2000b; Borradaile and Hamilton, 2003; Lagroix and Borradaile, 2000].

[54] The SC plot earned rigorous scientific meaning when physical rationale was provided [Tauxe et al., 2002]. The SC plot is advantageous over the Day plot in two senses. First, the SC plot can clearly diagnose not only grain size but also dominant anisotropy. Second, the SC plot is easier to obtain because B_{cr} determination is not needed. Note that determination of B_{cr} from the hysteresis loop directly rather than from a separate back-field

experiment is often ambiguous and has yielded different outcomes depending on the experimental procedures [von Dobeneck, 1996; Fabian and von Dobeneck, 1997].

[55] It is surprising that an SC plot without B_{cr} measurements offers much more information than a Day diagram (Figures 4, 6, 8, 10, 12, and 15). This is particularly noticeable when hysteresis results were compiled for all grain sizes of synthetic samples (Figures 4 and 10). A clear dichotomy between ZFC and FC results disappears on a Day diagram (Figures 10c and 10d). A difference between titanomagnetite- and magnetite-bearing samples is better resolved in an SC plot (Figure 4). The effects of volume concentration and FC/ZFC are also better recognized in SC plots (Figure 8). Why is the Day plot disadvantaged? It is because B_c and B_{cr} share a similar temperature dependence. When their ratios are used, the Day plot masks important rock magnetic information.

5. Conclusions

[56] Magnetic hysteresis has been used as a primary indicator of domain state in magnetic samples. Temperature dependence of magnetic hysteresis has been investigated to better constrain the dominant anisotropy and changes of domain state at various temperatures. For the magnetite-bearing samples used in this study, hysteresis properties were mainly controlled by shape anisotropy in most temperature ranges. However, other competing anisotropies contributed at two different temperature ranges. At temperature intervals below 120 K, magnetocrystalline anisotropies are mostly responsible for the significant increase of B_c and M_r . A strong magnetostrictive anisotropy is responsible for quite different hysteretic behavior of titanomagnetite-bearing samples.

Acknowledgments

[57] Jeff S. Gee generously donated a large collection of MORBs for use in this study. We thank Mike Jackson, Jim Marvin, and Peat Solheid of the Institution for Rock Magnetism (IRM) for their help with the measurements. Funding for the IRM is provided by the Keck Foundation, the National Science Foundation, Earth Sciences Division, and the University of Minnesota. Dennis Kent and two anonymous referees

provided helpful reviews. This research was supported by NSF grant EAR0229498 to L. Tauxe and N. Bertram.

References

- Abe, K., Y. Miyamoto, and S. Chikazumi (1976), Magneto-crystalline anisotropy of low-temperature phase of magnetite, *J. Phys. Soc. Jpn.*, *41*(6), 1894–1902.
- Argyle, K., and D. J. Dunlop (1990), Low-temperature and high-temperature hysteresis of small multidomain magnetites (215–540 nm), *J. Geophys. Res.*, *95*, 7083–7096.
- Baruchel, J., E. Boller, J. I. Espeso, H. Klein, C. Medrano, J. Nogues, E. Pernot, and M. Schlenker (2001), Bragg-diffraction imaging of magnetic crystals with third-generation synchrotron radiation, *J. Magn. Magn. Mater.*, *233*, 38–47.
- Beske-Diehl, S., and W. L. Soroka (1984), Magnetic properties of variably oxidized pillow basalts, *Geophys. Res. Lett.*, *11*, 217–220.
- Bina, M. M., and M. Prevot (1989), Thermomagnetic investigations of titanomagnetite in submarine basalts: Evidence for differential maghemitization, *Phys. Earth Planet. Inter.*, *54*, 169–179.
- Borradaile, G. J., and T. Hamilton (2003), Limestones distinguished by magnetic hysteresis in three-dimensional projections, *Geophys. Res. Lett.*, *30*, 1973, doi:10.1029/2003GL017892.
- Borradaile, G. J., and F. Lagroix (2000a), Magnetic fabric interpretation complicated by inclusions in mafic silicates, *Tectonophysics*, *325*, 217–225.
- Borradaile, G. J., and F. Lagroix (2000b), Tectonics of the Circum-Troodos sedimentary cover of Cyprus, from rock magnetic and structural observations, *J. Struct. Geol.*, *22*, 453–469.
- Carlut, J., and D. V. Kent (2002), Grain size dependent paleointensity results from very recent mid-oceanic ridge basalts, *J. Geophys. Res.*, *107*(B3), 2049, doi:10.1029/2001JB000439.
- Carter-Stiglitz, B., M. Jackson, and B. M. Moskowitz (2002), Low-temperature remanence in stable single domain magnetite, *Geophys. Res. Lett.*, *29*(7), 1129, doi:10.1029/2001GL014197.
- Dankers, P. (1981), Relationship between median destructive field and remanent coercive force for dispersed natural magnetite, titanomagnetite, and hematite, *Geophys. J. R. Astron. Soc.*, *64*, 447–461.
- Dankers, P., and N. Sugiura (1981), The effects of annealing and concentration on the hysteresis properties of magnetite around the psd-md transition, *Earth Planet. Sci. Lett.*, *56*, 422–428.
- Day, R., M. Fuller, and V. A. Schmidt (1977), Hysteresis properties of titanomagnetites: Grain size and composition dependence, *Phys. Earth Planet. Inter.*, *13*, 260–267.
- Dunlop, D. J. (1977), The coercive force spectrum of magnetite at high temperatures: Evidence for thermal activation below the blocking temperature, *Geophys. J. R. Astron. Soc.*, *51*, 121–147.
- Dunlop, D. J. (1987), Temperature dependence of hysteresis in 0.04–0.22 μm magnetites and implications for domain structure, *Phys. Earth Planet. Sci.*, *46*, 100–119.

- Dunlop, D. J. (2002a), Theory and application of the Day plot: 1. Theoretical curves and tests using titanomagnetite data, *J. Geophys. Res.*, *107*(B3), 2056, doi:10.1029/2001JB000486.
- Dunlop, D. J. (2002b), Theory and application of the Day plot: 2. Application to data for rocks, sediments, and soils, *J. Geophys. Res.*, *107*(B3), 2057, doi:10.1029/2001JB000487.
- Dunlop, D. J., P. W. Schmidt, O. Özdemir, and D. A. Clark (1997), Paleomagnetism and paleothermometry of the Sydney Basin: 1. Thermoviscous and chemical overprinting of the Milton Monzonite, *J. Geophys. Res.*, *102*, 27,271–27,283.
- Fabian, K. (2003), Some additional parameters to estimate domain state from isothermal remanent magnetization, *Earth Planet. Sci. Lett.*, *213*, 337–345.
- Fabian, K., and T. von Dobeneck (1997), Isothermal magnetizations of samples with stable Preisach function: A survey of hysteresis, remanence, and rock magnetic parameters, *J. Geophys. Res.*, *102*, 17,659–17,677.
- Fletcher, E. J., and W. O'Reilly (1974), Contribution of Fe^{2+} ions to the magnetocrystalline anisotropy constant K_1 of $Fe_3 - xTi_xO_4$, $0 < x < 0.1$, *J. Phys. C Solid State Phys.*, *7*, 171–178.
- Gee, J. S., and D. V. Kent (1995), Magnetic hysteresis in young mid-ocean ridge basalts: Dominant cubic anisotropy?, *Geophys. Res. Lett.*, *22*, 551–554.
- Gee, J. S., and D. V. Kent (1999), Calibration of magnetic granulometric trend in oceanic basalts, *Earth Planet. Sci. Lett.*, *170*, 377–390.
- Hartstra, R. L. (1982a), A comparative study of the ARM and Irs of some natural magnetites of MD and PSD grain size, *Geophys. J. R. Astron. Soc.*, *71*, 497–518.
- Hartstra, R. L. (1982b), Grain-size dependence of initial susceptibility and saturation magnetization-related parameters of four natural magnetites in the PSD-MD range, *Geophys. J. R. Astron. Soc.*, *71*, 477–495.
- Heider, F. L., D. J. Dunlop, and N. Sugiura (1987), Magnetic properties of hydrothermally recrystallized magnetite crystals, *Science*, *236*, 1287–1290.
- Hodoch, J. P. (1990), Magnetic hysteresis as a function of low temperature in rocks: Evidence for internal stress control of remanence in multidomain and pseudo-single-domain magnetites, *Phys. Earth Planet. Inter.*, *64*, 21–36.
- Hodoch, J. P., R. I. Mackay, and G. M. English (1998), Low-temperature demagnetization of saturation remanence in magnetite-bearing dolerites of high coercivity, *Geophys. J. Int.*, *132*, 401–411.
- Kakol, Z., J. Sabol, and J. M. Honig (1991), Magnetic anisotropy of titanomagnetites $Fe_3 - xTi_xO_4$, $0 < x < 0.55$, *Phys. Rev. B*, *44*, 2198–2204.
- Keller, R., and E. Schmidbauer (1999), Magnetic hysteresis properties and rotational hysteresis losses of synthetic stress-controlled titanomagnetite particles: 1. Magnetic hysteresis properties, *Geophys. J. Int.*, *138*, 319–333.
- Kent, D. V., and J. S. Gee (1996), Magnetic alteration of zero-age oceanic basalt, *Geology*, *24*, 703–706.
- Klapel, G. D., and P. N. Shive (1974), High-temperature magnetostriction of magnetite, *J. Geophys. Res.*, *79*, 2629–2633.
- Kosterov, A. (2001), Magnetic hysteresis of pseudo-single-domain and multidomain magnetite below the Verwey transition, *Earth Planet. Sci. Lett.*, *186*, 245–253.
- Kosterov, A. (2002), Low-temperature magnetic hysteresis of partially oxidized magnetite, *Geophys. J. Int.*, *149*, 796–804.
- Lagroix, F., and G. J. Borradaile (2000), Magnetic characterization using a 3-D hysteresis projection, illustrated with a study of limestone, *Geophys. J. Int.*, *141*, 213–226.
- Lanci, L., and D. V. Kent (2003), Introduction of thermal activation in forward modeling of hysteresis loops for single-domain magnetic particles and implications for the interpretation of the Day diagram, *J. Geophys. Res.*, *108*(B3), 2142, doi:10.1029/2001JB000944.
- Levi, S., and R. T. Merrill (1978), Properties of single-domain, pseudo-single-domain, and multidomain magnetite, *J. Geophys. Res.*, *83*, 309–323.
- Lowrie, W., and D. V. Kent (1969), Effect of annealing on coercive force and remanent magnetization in magnetite, *J. Geophys. Res.*, *74*, 2698–2710.
- Medrano, C., M. Schlenker, J. Baruchel, J. Espeso, and Y. Miyamoto (1999), Domains in the low-temperature phase of magnetite from synchrotron radiation x-ray topographs, *Phys. Rev. B*, *59*, 1185–1195.
- Moloni, K., B. M. Moskowitz, and E. D. Dahlberg (1996), Domain structures in single crystal magnetite below the Verwey transition as observed with a low-temperature magnetic force microscope, *Geophys. Res. Lett.*, *23*, 2851–2854.
- Moskowitz, B. M. (1993), High-temperature magnetostriction of magnetite and titanomagnetites, *J. Geophys. Res.*, *98*, 18,011–18,026.
- Moskowitz, B. M., R. B. Frankel, and D. A. Bazylinski (1993), Rock magnetic criteria for the detection of biogenic magnetite, *Earth Planet. Sci. Lett.*, *120*, 288–300.
- Moskowitz, B. M., R. B. Frankel, S. A. Walton, D. P. E. Dickson, K. K. W. Wong, T. Douglas, and S. Mann (1997), Determination of the preexponential frequency factor for superparamagnetic maghemite particles in magnetoferritin, *J. Geophys. Res.*, *102*, 22,671–22,680.
- Moskowitz, B. M., M. Jackson, and C. Kissel (1998), Low-temperature magnetic behavior of titanomagnetites, *Earth Planet. Sci. Lett.*, *157*, 141–149.
- Muxworthy, A. R. (1999), Low-temperature susceptibility and hysteresis of magnetite, *Earth Planet. Sci. Lett.*, *169*, 51–58.
- Özdemir, O. (2000), Coercive force of single crystals of magnetite at low-temperatures, *Geophys. J. Int.*, *141*, 351–356.
- Özdemir, O., and W. O'Reilly (1981), High-temperature hysteresis and other magnetic properties of synthetic monodomain titanomagnetites, *Phys. Earth Planet. Inter.*, *25*, 406–418.
- Özdemir, O., and W. O'Reilly (1982), Magnetic hysteresis properties of synthetic monodomain titanomagnetites, *Earth Planet. Sci. Lett.*, *57*, 437–447.
- Özdemir, O., D. J. Dunlop, and B. M. Moskowitz (2002), Changes in remanence, coercivity, and domain state at low temperature in magnetite, *Earth Planet. Sci. Lett.*, *194*, 343–358.

- Pick, T., and L. Tauxe (1993), Geomagnetic paleointensities during the Cretaceous normal super chron measured using submarine basaltic glass, *Nature*, *366*, 238–242.
- Sahu, S., and B. M. Moskowitz (1995), Thermal dependence of magnetocrystalline anisotropy and magnetostriction constants of single crystal $Fe_{2.4}Ti_{0.6}O_4$, *Geophys. Res. Lett.*, *22*, 449–452.
- Schmidbauer, E., and R. Keller (1994), Magnetic properties and rotational hysteresis of a basalt with homogeneous Ti-rich titanomagnetite grains 10–20 μm in diameter, *Geophys. J. Int.*, *119*, 880–892.
- Schmidbauer, E., and R. Keller (1996), Magnetic properties and rotational hysteresis of magnetite and maghemite particle 250 nm in diameter, *J. Magn. Magn. Mater.*, *152*, 99–108.
- Schmidbauer, E., and N. Schembera (1987), Magnetic hysteresis properties and anhysteretic remanent magnetization of spherical magnetite particle in the grain range 60–160 nm, *Phys. Earth Planet. Inter.*, *46*, 77–83.
- Smirnov, A. V., and J. A. Tarduno (2002), Magnetic field control of the low-temperature magnetic properties of stoichiometric and cation-deficient magnetite, *Earth Planet. Sci. Lett.*, *194*, 359–368.
- Stoner, E. C., and E. P. Wohlfarth (1948), A mechanism of magnetic hysteresis in heterogeneous alloys, *Philos. Trans. R. Soc. London, Ser. A*, *240*, 599–642.
- Syono, Y., and Y. Ishikawa (1963), Magnetocrystalline anisotropy of $xFe_2TiO_4 - (1 - x)Fe_3O_4$, *J. Phys. Soc. Jpn.*, *18*, 1230–1231.
- Tauxe, L., and J. Love (2003), Paleointensity in Hawaiian Scientific Drilling Project Hole (HSDP2): Results from submarine basaltic glass, *Geochem. Geophys. Geosyst.*, *4*(2), 8702, doi:10.1029/2001GC000276.
- Tauxe, L., A. T. Mullender, and T. Pick (1996), Pot-bellies, wasp-waists and superparamagnetism in magnetic hysteresis, *J. Geophys. Res.*, *101*, 571–583.
- Tauxe, L., H. N. Bertram, and C. Seberino (2002), Physical interpretation of hysteresis loops: Micromagnetic modeling of fine particle magnetite, *Geochem. Geophys. Geosyst.*, *3*(10), 1055, doi:10.1029/2001GC000241.
- Tucker, P. (1981), Low-temperature magnetic hysteresis properties of multidomain single-crystal titanomagnetites, *Earth Planet. Sci. Lett.*, *54*, 167–172.
- von Dobeneck, T. (1996), A systematic analysis of natural remanent magnetic mineral assemblages based on modeling hysteresis loops with coercivity-related hyperbolic basis function, *Geophys. J. Int.*, *124*, 675–694.
- Xu, W., R. van-der Voo, and D. R. Peacor (1998), Electron microscopic and rockmagnetic study of remagnetized Leadville carbonates, central Colorado, *Tectonophysics*, *196*, 333–362.
- Yu, J., D. J. Dunlop, and O. Özdemir (2002), Partial anhysteretic remanent magnetization in magnetite: 1. Additivity, *J. Geophys. Res.*, *107*(B10), 2244, doi:10.1029/2001JB001249.
- Yu, Y. (1998), Rock magnetic and paleomagnetic experiments on hemoilmenites and titanomagnetites in some volcanic rocks from Japan, M.Sc., Univ. of Toronto, Toronto, Canada.
- Yu, Y., and D. J. Dunlop (2001), Paleointensity determination on the late precambrian Tudor Gabbro, Ontario, *J. Geophys. Res.*, *106*, 26,331–26,344.
- Yu, Y., and D. J. Dunlop (2002), Multivectorial paleointensity determination from the Cordova Gabbro, southern Ontario, *Earth Planet. Sci. Lett.*, *203*, 983–998.